Polymeric membranes with selective permeability: shielding of an antioxidant enzyme

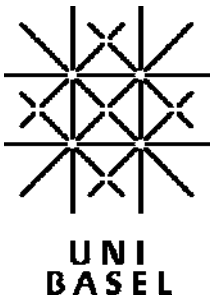

Inauguraldissertation

zur

Erlangung der Würde eines Doktors der Philosophie

vorgelegt der Philosophisch-Naturwissenschaftlichen Fakultät der

Universität Basel

von

Fabian Axthelm

aus Zangenberg/ Deutschland

Basel/ 2008

Genehmigt von der Philosophisch-Naturwissenschaftlichen Fakultät

auf Antrag von

Prof. Dr. Wolfgang Meier (Universität Basel)

und

Prof. Dr. Ulrich Schwaneberg (Jacobs University/ Bremen)

Basel, den 24. Mai 2008

Prof. Dr. Hans-Peter Hauri

Dekan

to Kerstin & Hannah

Abstract

In this work we designed an antioxidant nanoreactor based on the encapsulation of CuZnSOD in amphiphilic copolymer nanovesicles. The nanovesicles are formed by self-assembly of amphiphilic copolymer poly-(2-methyloxazoline)-poly-(dimethylsiloxane)-poly-(2-methyloxazoline) (PMOXA-PDMS-PMOXA). We chose this polymer due to its advantages over conventional systems, i.e. liposomes. Polymer nanocontainers can be produced with a controlled mean diameter and low polydispersity compared to liposomes. They were tested and shown to be more stable than liposomes.[1] These represent the main advantages with respect to the application as carriers to improve the drug stability and the circulation life-time. Another factor which could increase dramatically the circulation life-time and therefore the availability of the encapsulated SOD, is the stealth property of the poly-(2-methyloxazoline) chain, comparable to that of PEG. Besides, the polymer used for this study, has an oxygen permeable membrane, as will be shown later. All these advantages make the nanoreactors a completely new approach of drug delivery systems, in which the cargo is not released, but performs its function within the vesicle.

The nanovesicles, made of poly-(2-methyloxazoline)-poly (dimethylsiloxane)-poly (2-methyloxazoline), successfully encapsulated the SOD protein during their formation by a self-assembling process, as proved by confocal laser-scanning microscopy and fluorescence-correlation spectroscopy. Electron paramagnetic resonance spectroscopy and circular dichroism analyses showed that no structural changes appeared within the proteins once inside the inner cavity of the nanovesicles. The function of this antioxidant nanoreactor was tested by pulse radiolysis which demonstrated that superoxide dismutase remains active inside the nanovesicles.

This simple and robust hybrid system provides selective shielding of a sensitive enzyme from proteolytic attack and therefore points to a new direction for developing drug delivery applications.

Table of contents

List of abbrevations

% *percent*

°C *degree celsius*

Å *Angstrom*

A_2 *second virial coefficient*

a_i *proportion of i in the total core solution*

AmpR *amplex red*

Ar *Argon*

CD *circular dichroism*

CLSM *confocal laser scanning microscopy*

CMC *critical micelle concentration*

cpm *counts per molecule*

cpm_i *individual molecular brightness*

cpm_T *total molecular brightness*

CuZnSOD *copper-zinc superoxide dismutase*

D *diffusion coefficient*

DLS *dynamic light scattering*

EPR *electron paramagnetic resonance*

EPR effect *enhanced permeability and retention*

FCS *fluorescence correlation spectroscopy*

GSH *gluthatione*

GSSG *gluthatione disulphide*

He-Ne *Helium-Neon*

HRP *horseradish peroxidase*

k_b *Boltzmann constant*

kDa *kilo Dalton*

kHz *kilo Herz*

LCST *lower critical solution temperature*

M *weight-average molar mass*

ms *millisecond*

mW *milli Watt*

nm *nanometer*

PDI *polydispersity*

PEG *polyethylene glycol*

P_L *laser power*

PMOXA-PDMS-PMOXA *poly-(2-methyloxazoline)-poly-(dimethylsiloxane)-poly-(2-methyloxazoline)*

R_g *radius of gyration*

R_H *hydrodynamic radius*

RNS *reactive nitrogen species*

ROS *reactive oxygen species*

s *second*

SLS *static light scattering*

SOD *Superoxide dismutase*

T *temperature*

TEM *transmission electron microscopy*

u/mL *units/mL*

z-average *average particle diameter*

η *viscosity*

λ_{em} *emission wavelength*

λ_{ex} *excitation wavelength*

λ *wavelength*

□s *micro second*

□$_d$ *diffusion time*

1 Introduction

The formulation of pharmaceuticals in drug delivery systems is most challenging, since delivery of a broad range of pharmaceuticals with different mode of actions, as well as biological and chemical properties, can cause undesired side effects in the human body. Furthermore, a multitude of different conditions in the body interfere with the delivery of pharmaceuticals to their target, and have a negative impact on drug stability.

Drug delivery systems have to match various requirements with respect to the efficiency of a specific drug: (1) to enable the application of pharmaceutically active compounds e.g. by increasing their solubility, (2) to protect their cargo from unwanted reactions in the human body, e.g. degradation, gastrointestinal irritation, (3) to prevent from unwanted side reactions with physiological pathways and organs, and (4) to deliver the drug to its site of action.

To reach all these aims, a variety of strategies has been developed. Nanocontainers, often based on lipid- or polymer vesicles or micelles, and drug-polymer conjugates are employed to carry pharmaceuticals. The drugs stay protected due to their local separation from the environment. Besides, the nanocarrier can be functionalized to support specific delivery within the human body. The development of new biocompatible materials for drug delivery systems is a crucial factor, since the increasing number of new biopharmaceuticals with specific mode of action demand a broad portfolio of formulation possibilities. In this study we focus on the application of polymer-based vesicles. Polymers offer the unique possibility to be controlled in their behavior by their chemistry and architecture, which opens a perspective to create nano-sized objects to be applied in bio- and pharmaceutical sciences.

1.1 Polymers and block copolymers

1.1.1 Definitions

The word 'polymer' derives from Greek, where *poly* means “many” and *meros* means “part”. They consist of repeating units called monomers, which are covalently connected to give high molecular weight compounds. Due to their architecture, they can be classified into linear or branched polymers and dendrimers (Figure 1). Dendrimers are a special class of branched polymers, which are marked out by branched branches.

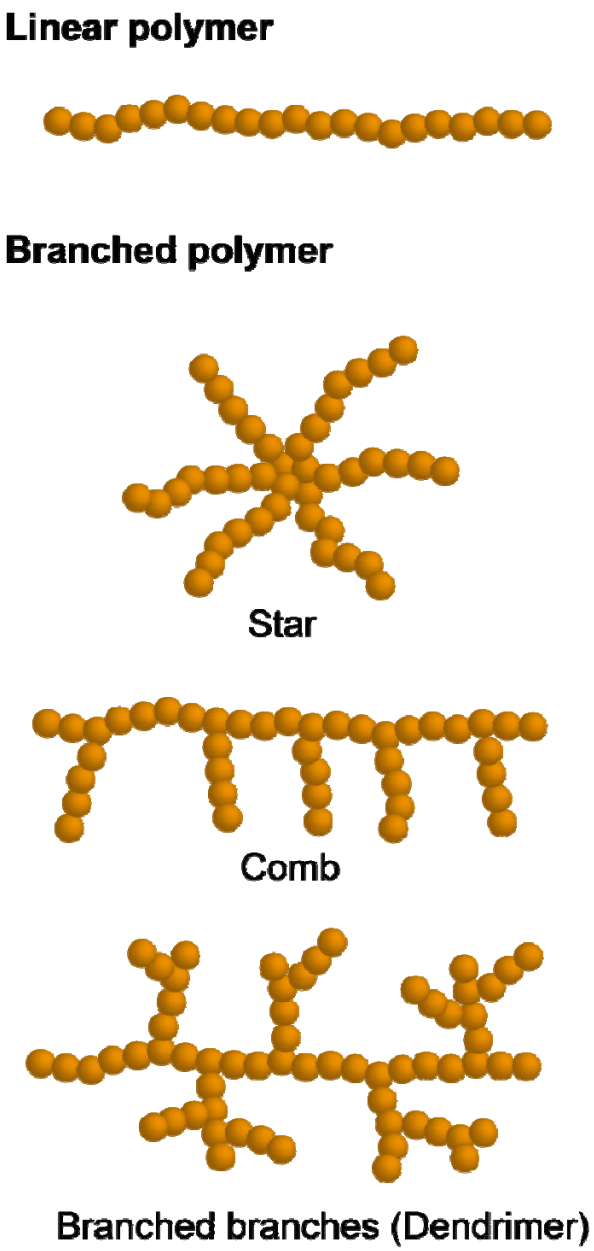

Figure 1 Schematic drawing of different polymer architectures.

Further classifications can be made, depending on the chemical nature of the monomers which form the polymeric chain. Polymers with only one type of monomers are called homopolymers (Figure 2). If two different monomers are present in one polymer chain, the term copolymer is used. The sequence, in which different repeating units appear in copolymers leads to further differentiation.

Polymers containing alternating monomers are called alternating copolymers (Figure 2), while those containing monomers which do not alternate periodically are described as random copolymers. If different monomers are grouped together, they form blocks, and the polymer built after covalent linking of such blocks is then termed a block copolymer (Figure 2).

Block-copolymers consist of at least two, covalently bound segments or blocks of different homopolymers. A diblock-copolymer can have a general form of A_nB_m, with A and B standing for different monomers and n and m giving the degree of polymerization (Figure 2). A further differentiation of block-copolymers can be made by taking the physico-chemical properties of the blocks into account, such as hydrophilicity and hydrophobicity. Polymers, which contain hydrophilic and hydrophobic blocks covalently linked together, are named amphiphilic block-copolymers.

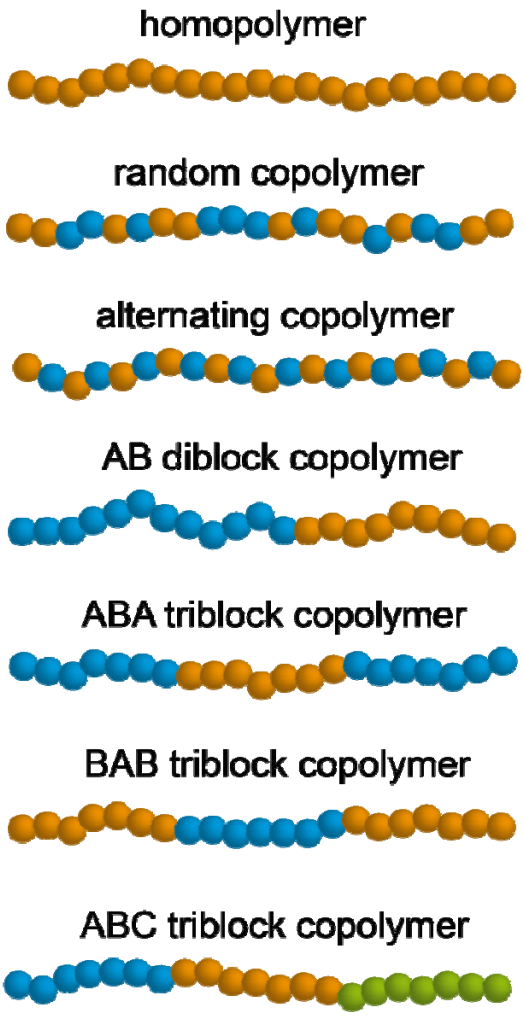

Figure 2 Schematic representation of linear polymers.

1.1.2 Self-assembly of block copolymers

Self-assembly is defined as the spontaneous building up of complex structures from the components of the system, by noncovalent forces. The transition from a disordered to an ordered phase can be induced by changing thermodynamic or physical parameters, such as temperature, chemical potential (concentration, pH value, salt concentration), mechanical fields (pressure, shear, extension, ultrasonic field), as well as electric or magnetic fields. The ordered state can be distinguished by e.g. the location of molecules at restricted three-dimensional regions. Transferred

to the topic of polymer sciences the self-assembly process can be described as interplay of different forces, e.g. long-range repulsive forces (e.g. hydrophilic-hydrophobic), short-range attractive (covalent binding of polymeric blocks) forces, chemical or physical incompatibility. One feasibility of self assembly, due to the mentioned forces, are short-range attractive and long-range repulsive forces (Figure 3A). Both blocks, hydrophilic and hydrophobic, of an amphiphilic block copolymer are covalently linked together. This linkage represents the short-range attractive forces, forcing both blocks to stay together. The long range repulsive forces are caused by reciprocal repulsion of the hydrophilic and the hydrophobic block. This contrary forces within one molecule, which can't be avoided, lead to the formation of self assembled structures of structures.

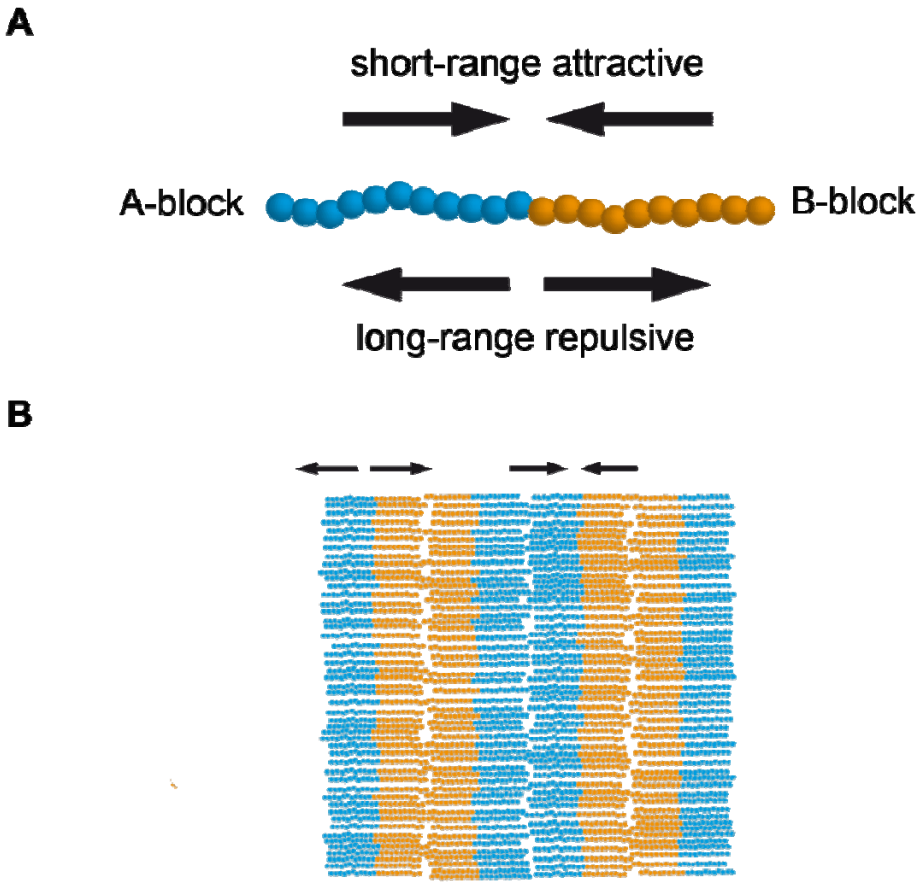

Figure 3 A) Illustration of long-range repulsive and short-range attractive forces leading to B) example of self-organization (with arrows marking short-range attractive and long-range repulsive forces).

Self-assembly of amphiphilic block copolymers in solution can be controlled by taking into account several parameters, which induce the directed formation of different morphologies, e.g. spheres, rods, lamellae and vesicles. It has been found, that the formation of different morphologies (Figure 4) is a function of the total and relative block lengths, temperature, chemical nature of each block, type of solvent, and concentration.[2, 3] One special feature of block copolymer chemistry is the versatility of their chemistry to ensure the right chemical composition, length and structure of the constituting blocks in order to tune the association characteristics and thus the

obtained morphologies. Moreover, by changing the architecture of the blocks different mesophases can be achieved.

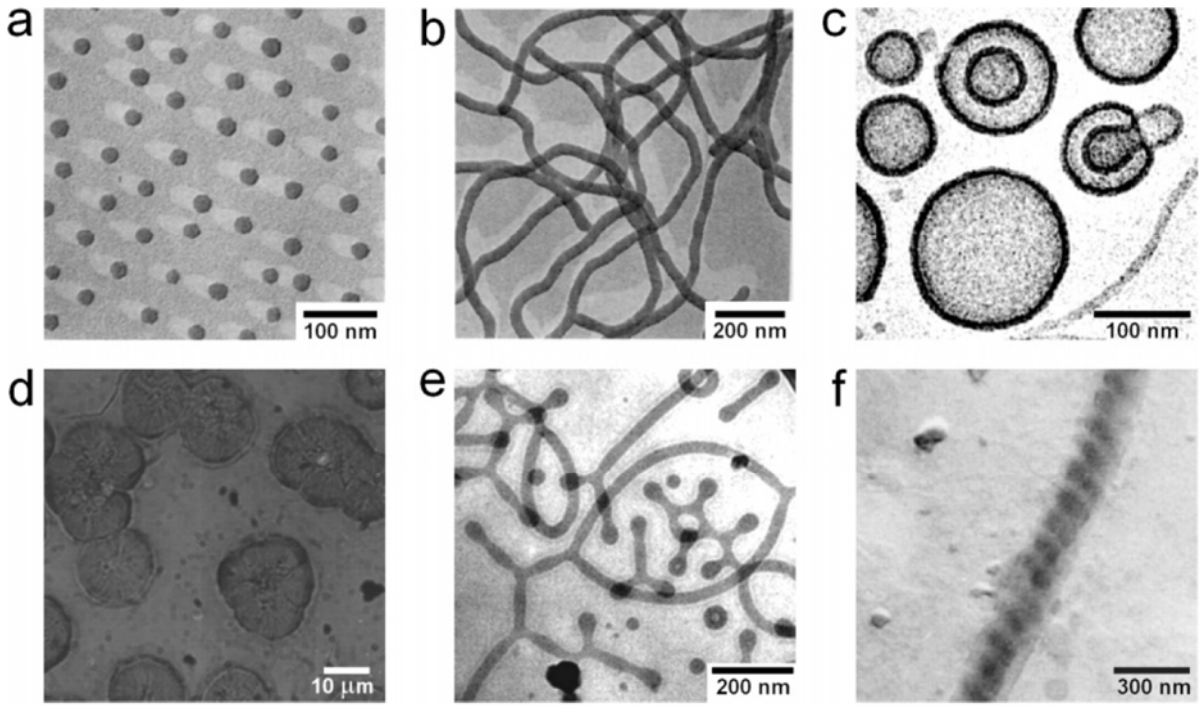

Figure 4 Transmission electron micrographs of various types of morphologies formed by aggregated block copolymers. a) spherical micelles and b) rod-like micelles from polystyrene-b-poly(acrylic acid), c) vesicles from poly(ethylene oxide)-b-polyethylethylene, d) lamellae from polystyrene-b-poly(phenylquinoline), e) branched worm-like micelles from poly(ethylene oxide)-b-polybutadiene, and f) left-hand helices from polystyrene-b-poly(L-isocyanoalanyl-L-alanine).[4]

In the context of drug delivery systems, the most interesting self-assembled structures obtained from block copolymers are micelles (Figure 5) and vesicles. Self-assembly occurs by exceeding a critical aggregation concentration.[5, 6]

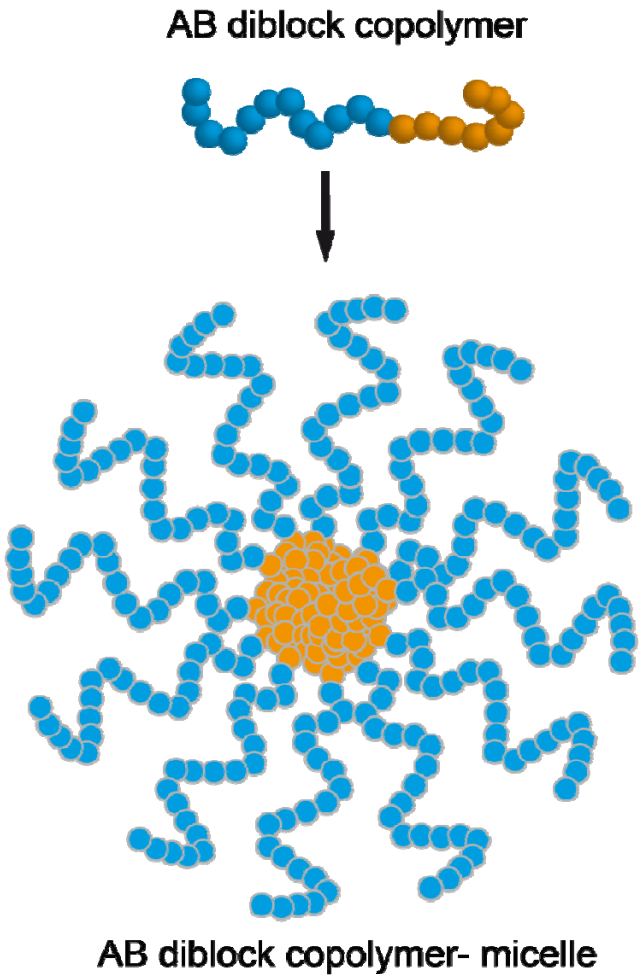

Figure 5 Scheme of a micelle made from a diblock copolymer

In aqueous solution, micellization occurs above the critical micelle concentration by selective solubilization of the hydrophilic block, while the core is formed by the hydrophobic block. Slower dynamics of the constituent blocks [7, 8] makes block copolymer micelles more stable compared to lipid micelles. The stability, which is a function of the intermicellar chain exchange[1] is mainly dependent on the type of blocks, e.g. their relative polarity, the overall chain length and the relative block length, and can be tailored to be very small in contrast to lipid micelles. Therefore, self-assembled structures based on block copolymers show higher structural stability.

[1] ability of micelles to coalesce and redistribute

Depending on the asymmetry of the constituting blocks, micellar structures can be classified as star- and crew-cut micelles (Figure 6). The aggregates are called star micelles, if the corona-forming block (block exposed to the solvent) is much longer than the core-forming block.[9, 10] If the corona-forming block is much shorter than the core-forming block, the aggregates are called crew-cut micelles.[11-13]

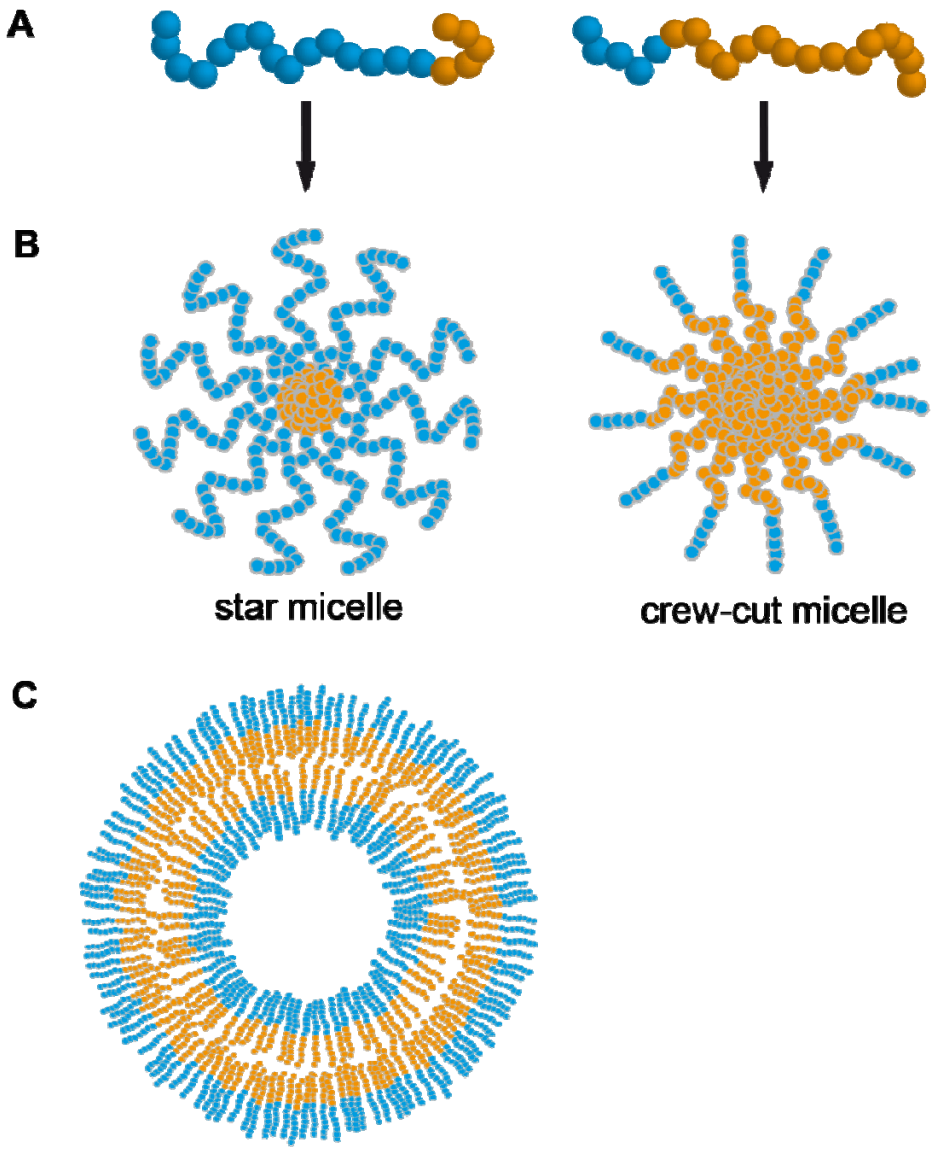

Figure 6 A) A schematic representation of AB diblock copolymer unimers. B) Depending on the ratio of hydrophilic and hydrophobic blocks, the unimers can form

star- or crew-cut micelles. C) AB diblock copolymers can also self-assemble into vesicular structures.

Diblock copolymers with long hydrophilic chains tend to form micellar aggregates due to the highly positive curvature of the interface. As the length of the insoluble block increases, the curvature decreases and a transition to rod-like micelles is observed. If the length of the insoluble block increases further, lamellar phases are favored. Depending on the water concentration, lamellae can swell to a point, where the balance of hydrophilic and hydrophobic forces changes and the membrane rearrange to nonpolar configurations. Additional parameters, which control this rearrangements is the stiffness and the molecular properties of the membrane.

Vesicles have been present since the first cell existed, and play a critical role in compartmentalization functions, such as transport and biological protection. Due to the material vesicles are built from, they are named differently. Vesicles made of lipids, which are natural amphiphiles, well known for their ability to self-assemble, are named liposomes. Vesicles based on polypeptides, named peptosomes, are reported to support the function of biocompatibility.[14-16] Polypeptides are prone to hydrolysis, as already widely exploited in the field of controlled drug release. Natural and synthetic amphiphilic polymers can generate vesicles in various media, ranging from organic solvents to pure aqueous solution. These polymer vesicles are called polymersomes, and are of big scientific interest, due to their tunable properties which make them very versatile.

1.1.3 Polymersomes

Polymersomes are well-defined nano- or micrometer-sized objects (Figure 7). They can be desirable for various applications and therefore material science and nanotechnology pay special attention to the development of self-assembling materials. Made of amphiphilic block copolymers, the polymersomes represent a special class of superstructures. Polymer chemistry offers - by engineering of block composition and block length - a great potential to design new materials well suited to mimic and replace biological macromolecules. Properties of polymer- and liposomes have been compared and it has been found that the polymer membrane shows less permeability for water and an increased stability.[6] In this respect, polymer vesicles are more versatile since their fluidity properties can be tailored by tuning the glass transition temperature of the constituting blocks. The diameter of polymersomes can range, as reported, from 100 nm to a few µm.[17]

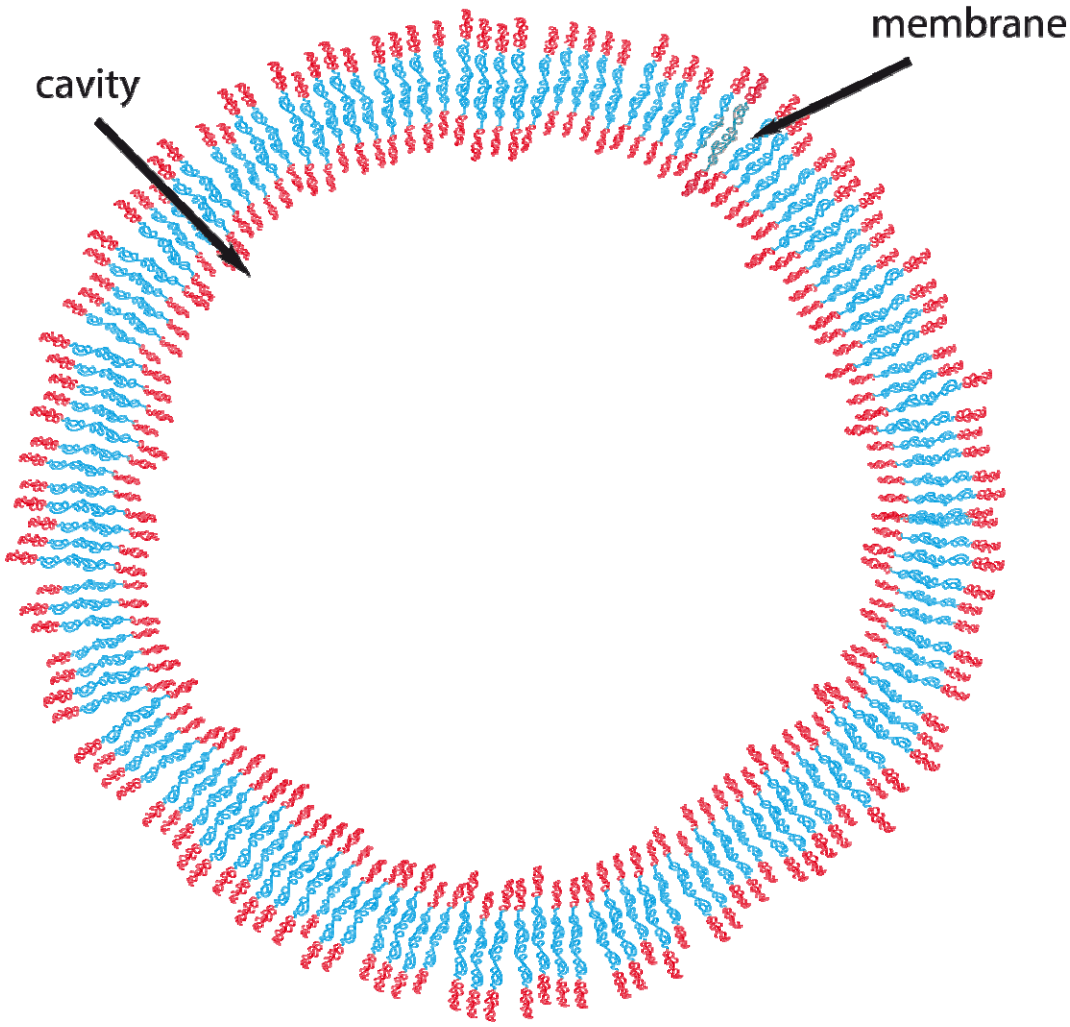

Figure 7 Sheme of a polymersome made from ABA triblock copolymer. The hollow sphere morphology can be used for various applications, such as drug delivery or reaction vessel.

Many research groups work on the development of new applications for polymersomes. Most of them are used to build compartments, which are a requirement in nature for the occurrence of many metabolic processes such as oxidation of fatty acids, the citrate cycle, and phosphorylation. Possible applications of polymersomes are transport and storage of compounds, chemical reactions of various compounds in situ, and targeting after functionalization of the vesicles'

surface. In the case of transport and storage, the hollow sphere morphology of the polymersomes serves to encapsulate agents, and therefore to protect sensitive compounds and to reduce the side effects caused by unspecific reactions.

Another advantage of polymersomes is the possibility to functionalize covalently their surface with different kinds of molecules, e.g. receptor-specific ligands [18] or cell penetrating peptides (CPPs).[19] In this way, they are directed to specific sites of action and are supported for cellular uptake. It was shown that properties of polymersomes can be triggered concerning their permeability, or stimuli-responsiveness (as for example pH, temperature, or light responsiveness).[20, 21]

1.1.4 Nanoreactors

In nature, almost all chemical conversions take place in a confined environment and are closely coupled to each other in such a way that the product of one reaction is the substrate or catalyst for the subsequent one. Such coupling of reactions in time and space is the fundament for highly developed processes in many organism. Influencing these processes demands a compartmentalization, too, and is therefore of growing interest for scientists.

Nanoreactors represent one possibility to approach the solution to this problem. Nanoreactors could be polymersomes, which are used for advanced applications in compartmentalization of chemical reactions. They must fulfill various requirements such as (1) efficient entrapment of the catalytic species, (2) stability and robustness to ensure protection of catalytic species, (3) selective diffusion of product molecules through the membrane, (4) no unwanted reaction to external influences (e.g. pH, ionic strength, temperature), and (5) the system must be innocuous to allow its use in living systems.[22]

Nanoreactors have been used in various applications as nanometer sized reaction vessel, e.g. by encapsulation of β-lactamase enzyme inside the water pool together with the incorporation of a channel protein into the polymer membrane.[23] Furthermore, the ability of nanocontainers was shown to mimic natural cells, as for example by the use of a channel protein as a receptor for λ phages. The channel protein triggered the ejection of the phage DNA into the inner cavity of the vesicle.[24]

1.1.5 Methods of polymersome preparation

Various methods of vesicle preparation are described in the literature. The following methods are the most conventional and are applied for the preparation of liposomes and polymersomes. They can be classified into methods using organic solvents and solvent-free methods.

In the first case, the membrane building molecules are dissolved in an organic solvent and mixed with an aqueous phase. A disadvantage of this method is that the solvent which remains in the sample leads to structural defects in the vesicle-forming membrane. Therefore, it needs to be extracted using appropriate methods (e.g. dialysis, biobeads).

The second method for polymersome preparation (film-rehydration) concerns the formation of vesicles starting from a dry state. The membrane forming material is dissolved in organic solvent and dried to a thin film at the inner surface of a vial. By further addition of an aqueous phase and application of mechanical energy (e.g. stirring) polydisperse vesicles are formed.

The polydispersity of the aggregates can be decreased by the application of further mechanical stress or force, such as extrusion. Using this technique, the vesicle size

and dispersity can be further decreased. For this purpose, the mixture is forced through a filter with a defined pore size. The shear force causes the break-down of the large vesicles and induces the formation of smaller and more monodisperse ones, depending on the filter pore size.

Another solvent-free method of vesicle preparation is accomplished by addition of detergents to a dry film of membrane building polymer. After addition of an aqueous phase, the detergent supports the shielding of the hydrophobic blocks from the aqueous phase. It is important, that the concentration of the detergent is above the critical micelle concentration (CMC)[2]. The detergent associated to the hydrophobic blocks is in equilibrium with the free detergent molecules in solution. By removal of the free detergent molecules the equilibrium adjusts, which induces a transition to vesicular structures. Several methods are known for removal of detergent, e.g. dilution [25] or biobeads [26].

1.1.6 Methods of characterization

Colloidal systems such as polymersomes can display variations in membrane properties and particle size and structure. Therefore methods for characterization are needed to evaluate particle size, number of lamellae, membrane formation and thickness. Especially the properties of the membrane are important for many applications and need to be known, such as permeability, elasticity, and charge of the surface. The most commonly used methods, and applied extensively in this work, are:

[2] The critical micelle concentration is the concentration of surfactants above which micelles are spontaneously formed.

- Light scattering is a phenomenon which is encountered in everyday life, like scattering of light by the particles in the atmosphere giving rise to the color of the sky. Light scattering enables the quantitative detection of the average particle diameter (z-average) and the polydispersity (PDI) of dispersed systems in a range between 5 and 1000 weight average molecular weight.

  The scattering of light by particles is based on their polarizability. Electrons of molecules interact with the oscillating electric field of radiation, which is inducing a dipole in the molecules which oscillates with the electric field. An oscillating dipole is a source of light, therefore the molecules emit scattered light, which is of the same wavelength as the incident radiation in the case of elastic scattering.

  The intensity of the scattered light is depending on the wavelength (λ) of the incident light, the particle size, and the angle at which the scattered light is measured. For small particles (λ >> diameter) the Rayleigh-approximation is valid. Small particles scatter incident light in all directions with the same intensity, which makes the measurement if the intensity of the radiated light independent from the angle. In case of bigger particles the intensity of scattered light is strongly dependent on the angle- maxima and minima of scattered light can be determined. Therefore bigger particles are always measured at various angles.

  Due to Brownian motion the particles move freely in solution, inducing concentration fluctuations and thus intensity fluctuations of the scattered light. These time-dependent fluctuations of the scattered light are detected. The movement of the particles is dependent on their size. Small particles move faster than bigger ones and therefore emit more scattering signals during time.

A monodisperse size distribution of particles in dispersion is unlikely. Therefore a complex signal of scattered light is detected and digitalized by an correlation software which calculate an autocorrelation function. Autocorrelation is a mathematical tool for finding repeating patterns of a signal by “comparing” the signal with itself. The autocorrelation function enables to extract the diffusion coefficient (D), which is related to the hydrodynamic radius (R_H) by the Stokes-Einstein equation. [27, 28]

$$D = \frac{k_b \cdot T}{6 \cdot \pi \cdot \eta \cdot R_H} \qquad \textit{Equation 1}$$

D- diffusion coefficient [m^2s^{-1}], k_b- Boltzmann constant [1,38 10^{-23} JK^{-1}], T-temperature [K], η- viscosity [Nsm^{-2}], R_H- hydrodynamic radius [m]

- Transmission electron microscopy (TEM) offers the possibility to visualize small objects in the nm size range. Related to vesicles this means, that vesicle size and size distribution can be investigated. With an electron microscope, much higher resolution can be reached than with a conventional light microscope, which is due to the smaller wavelength of electrons compared to light. The resolution achieved by electron microscopy is ~2 nm. In electron microscopy, a thin film of a sample is transilluminated by electrons and a two-dimensional picture of the sample can be obtained. During transillumination, various interactions between the electron beam and the sample take place. Interactions of the electrons with the nuclear envelope of the sample atoms cause the electron to emit energy in the wavelength of x-rays (10^{-12} m). This inelastic scattering, which gives spectroscopic information specific to the element, is filtered to increase the contrast. In the case of elastic scattering of the electrons on the atomic nuclei no energy loss is detected. The scattering

intensity of electrons with the atomic nuclei of the sample enables the contrast of the picture and increases with the atomic number. Therefore atoms with a low atomic number give a lower contrast. In electron microscopy, the sample thickness needs to be really low, in order to support the transillumination with electrons. In samples containing salt in the buffer solution the evaporation of the buffer can lead to local increase in salt concentration, which can cause artifacts. As the sample layer is really thin, bigger objects (> 400 nm) are often removed with excessive buffer. It should be always kept in mind, that high vacuum used in electron microscopy can cause shrinkage of the objects.

1.2 Drug delivery

The main function of drug delivery systems is the improvement of the therapeutic activity and safety. New therapeutics enter the market, e.g. oligonucleotides, genes, peptides and proteins, which have their own macromolecular properties and ask for new strategies to overcome physiological and physico-chemical barriers. For example, directly related to cancer therapy, such barriers can be (1) high interstitial fluid pressure (IFP), (2) reduced oxygen delivery (hypoxia), (3) low extracellular pH and (4) apoptosis resistance. Drug delivery systems are needed to maintain or change the macromolecular properties of pharmaceutically active compounds to overcome these barriers. The delivery of therapeutics by drug delivery systems can be an active or passive process. Additionally, drug delivery systems can both increase the bioavailability of therapeutics by strategies of controlled release, and minimize their adverse effects. Various drug delivery systems derived from the field of polymer sciences are continuously proposed to fit with the needs of new therapeutics. Their main advantage is the use of synthetic chemistry which allows

tailoring the polymers' molecular mass and additional biomimetic behavior, both important factors in drug delivery.

1.2.1 Polymer-conjugate strategies in drug delivery

Among the techniques used to develop new drug delivery systems, nanotechnology based on polymer chemistry, is very promising as it allows the control of polymer properties which are important for drug delivery, such as solubility, hydrophobicity and molecular mass. In this domain, mainly two systems are usually used: polymer conjugates and colloidal systems (micelles, liposomes, nanoparticles).

Polymer conjugates are often used to shield sensitive biopharmaceuticals such as enzymes. Enzymes as “molecular machines” play an important role in many metabolic processes in nature. A deficiency of an enzyme can cause profound consequences; a well-known example is insulin, which is part of the carbohydrate regulating machinery.

The use of polymer conjugates can efficiently reduce the immunogenicity, and therefore prolong the plasma half life, enhance stability and allow passive targeting of large molecular weight compounds. Polymer-based medicines have been used successfully for the treatment of cancer. Polymer-drug conjugate delivery in cancer therapy relies on the “enhanced permeability and retention effect” (EPR effect), a property which improves the accumulation of drugs in tumor tissue as compared to others.[29]

For example, covalent coupling of polyethylene glycol (PEG) (Figure 8) to amine groups of proteins prevents the proteins from recognition by the immune system. In addition, PEG modification facilitates the intracellular uptake of biopharmaceuticals, and elevates their intracellular activity. The increase of in vivo lifespan and

suppression of the immune response are proportional to the number and length of PEG molecules attached to a protein, but excessive modification compromises the activity.[30] PEG was shown to prolong the “half-lives” of modified proteins in the blood stream from a few minutes to several hours [31, 32] and to be able to preferentially localize at sites of inflammation.[33] No adverse side effects of PEG-modified enzymes have been reported to date.[34]

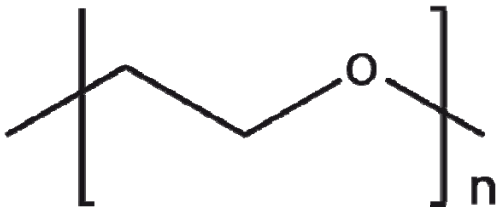

Figure 8 Chemical structure of poly(ethylene glycol)

- Another molecule known for its protective effect when used to modify biopharmaceuticals is chitosan (Figure 9), a hydrophilic, biocompatible and biodegradable polymer of low toxicity. Because of its bioadhesive and permeation enhanced properties, chitosan has received substantial attention in novel bioadhesive drug delivery systems, as it prolongs the residence time at the site of adsorption.[35] Several authors used chitosan-based polymers for liposome coating to increase stability towards drug release, or for targeting purposes.[36, 37]

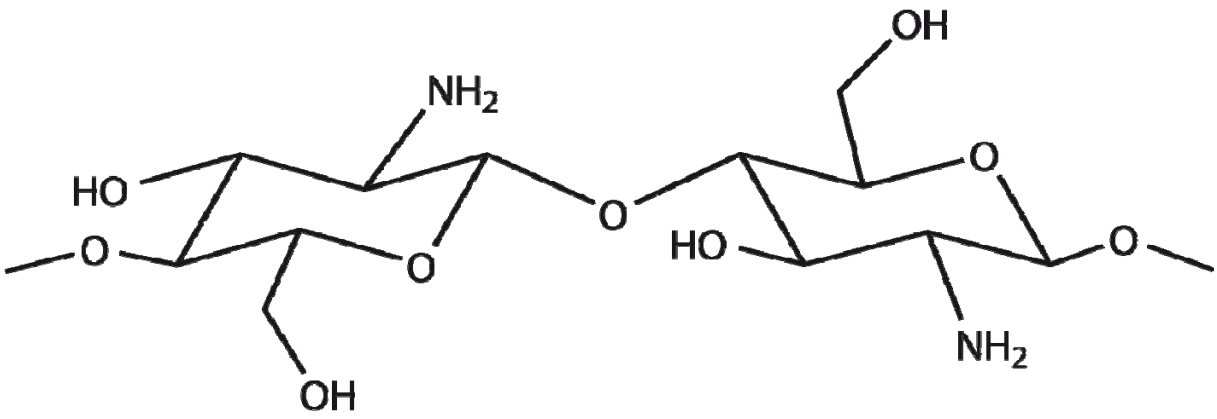

Figure 9 Chemical structure of chitosan

1.2.2 Polymeric carriers as a strategy for drug delivery

The encapsulation of compounds in carriers represents an important approach used in many areas of chemistry, pharmaceutics, and biotechnology. Different strategies have been developed and in this respect the use of colloidal systems such as micelles, liposomes and nanoparticles is well established.[33, 38, 39] Nevertheless, it is still a challenge for scientists to develop new constructs with the desired storage, targeting and/or release properties. The use of colloidal systems is characterized by the ability to enhance therapeutic activity and to reduce the toxicity of therapeutics, mainly by changing their pharmacokinetics and biodistribution.

Micelles represent a well studied and characterized drug delivery system, broadly reviewed in reference [40]. Numerous studies on the application of micelles were undertaken.[38, 41-44] The structural characteristics of polymeric micelles, their size and core-corona structure have some similarities to natural carriers like viruses and lipoproteins. The advantages of using polymeric micelles are (1) the support of long circulation, as the uptake by reticuloendothelial systems is lowered, (2) effective

prevention of non-specific adsorption of proteins and (3) the solubilization of hydrophobic drugs in the micellar core.

Liposomes as a drug delivery system represent one of the most conventional systems to protect biopharmaceuticals from degradation by the immune system. They were used in a wide variety of delivery approaches due to their property to facilitate intracellular delivery, via fusion with the plasma membrane, receptor-mediated endocytosis, and phagocytosis.[45] Encapsulation efficiency, size and surface (e.g. charge and rigidity) properties of the liposomes can be varied by the lipid composition and the preparation method. A various number of different preparation methods were tested for the encapsulation of proteins: dehydration-rehydration method,[46, 47] hydration of thin lipid film method,[47, 48] injection method,[49] reverse-phase evaporation and freeze-thawing method.[47] Different methods and lipid compositions give liposomes with different size distributions, lamellarity, encapsulation efficiencies and biological affinities. Modification of the outer surface of the liposomes with stealth and targeting moieties (e.g. PEG, chitosan) allows for their life span to be extended in vivo.

However, there are certain drawbacks of liposomes supporting the progress in polymer science, such as toxicity of cationic liposomes,[50, 51] structural defects causing leakage,[52] mechanical instability,[53] interactions with high-density lipoproteins,[54] and short blood circulation lifetime.[55]

- One of the most promising approaches for the design of drug delivery systems is the bottom-up design of polymeric systems using self-assembly mechanisms.[8, 56, 57] More than the liposomal systems, the use of polymeric carriers offers the control of physical and chemical properties, by changing the block length-ratio, or by introduction of functional groups. This makes them

more versatile for a wider range of applications.[58] In several studies, the mechanical properties of polymersome- and phospholipid membranes, such as area elastic and bending moduli, were compared and shown that polymersomes in the fluid state can be designed to be 5-50 times tougher than liposomes.[8]

A number of methods for the preparation of polymeric drug carriers are available. The selection of the method mainly depends on the chemical properties of the drug which needs to be formulated, hence for formulation of biomolecules, such as enzymes, solvent free methods are the first choice. For more hydrophobic molecules solvent-containing preparation methods can be used. All the methods follow the basic principle of vesicle preparation introduced in paragraph 1.1.5. In reference [59] a multitude of different methods for the formulation of biomolecules is discussed. Only a few general considerations for the selection of a specific preparation method are given at this point.

1.2.3 Directing pharmaceutically active compounds

Besides the need to maintain the stability and increase the bioavailability of pharmaceutical compounds, there is the need to deliver them to their specific site of action. Targeting can help lower the concentration of the administered drug as less drug is spreading in the organism, and therefore to decrease the probability of adverse effects. Two main strategies for the direction of drugs can be distinguished: passive and active targeting.

The passive targeting is accomplished by the properties of the carrier system and can be integrated during their design.

One example of passive targeting is the “enhanced permeability and retention” effect (EPR effect), which is connected to the use of polymer-drug conjugates. These conjugates showed enhanced bioavailability in vivo and a preferred uptake by carcinogenic tissues.

Another passive targeting approach is based on the use of stimuli-responsive systems. One example of passive targeting can be the use of pH-responsive carriers. Various diseases can cause changes in the pH in the near microenvironment. The pH-sensitive bonds, especially designed for polymer-drug conjugates can react on this change and cause the drug release.

Another way is to use thermosensitive carrier systems, which can mediate the release when temperature is increased above the phase transition temperature.[60] Thermally responsive drug-polymer conjugates were used to target solid tumors, due to the effect of hyperthermia.[61] In this approach, the carrier had lower critical solution temperature (LCST) between body temperature and the temperature in a tumor. This enables thermally targeted drug delivery by enhancing the localization of the thermally responsive drug carrier.

Active targeting is mostly accomplished by receptor-mediated delivery or the use of other biomolecules with highly specific affinity. For the receptor-mediated delivery, a specific ligand molecule, recognized by the receptor, is conjugated to a drug or a carrier. The conjugation of functional groups to the surface of polymersomes can be directly implemented in their design.[62] Antibodies directed against endothelial surface determinants, small antigen-binding fragments of these antibodies [62] and short peptidic signal sequences [19] represent the most useful approaches of surface modification of polymeric carriers. By binding of the ligand molecule to the receptor the process of internalization starts.[18]

Antibodies are naturally occurring biomolecules which help the body to fight infection. They can be exploited to target drugs to their site of action in the organism. Antibodies can be raised against a wide variety of proteins on the surface of tissues. Those surface proteins have several functions, important to maintain the metabolism of the tissue, but they can also serve as an indicator for diseases. Some diseases can cause changes of extracellular proteins exposed on the surface of the cell. When these changes are known, antibodies specific against these changed surface proteins can mediate drug targeting.[62]

1.2.4 Targets for drug delivery

The endothelium belongs to one of the most important therapeutic targets in living organism. The endothelium is the thin layer of cells which lines the interior surface of the blood vessels, forming an interface between circulating blood in the vessel and the vessel wall. Endothelial cells cover the whole interior surface of the circulatory system, from the heart to the smallest capillary. The endothelial cells are involved in important regulatory processes, e.g. vasoconstriction and vasodilation (control of blood pressure), thrombosis and fibrinolysis (control of blood clotting), atherosclerosis (chronic inflammatory disease in the wall of arteries) and inflammation. Table 1 shows selected candidate targets for drug delivery to endothelial cells. Furthermore the endothelium represents a barrier for drug delivery systems to reach the tissues beyond the vascular wall. Drug delivery systems with specific affinities, compatible with the endothelial binding sites, are needed to enhance the targeting and mediate internalization. Those specific affinities can be antibodies against endothelial surface proteins (Table 1). By binding to endothelial surface, proteins and receptors often cause internalization. The pathway for

internalization and possible transfer to other tissues is mainly dependent on the binding site / receptor. A summary of endocytic pathways is given in Figure 10. There are various pathways of internalization available in endothelial cells, such as clathrin- and caveoli-mediated endocytosis, phagocytosis, macropinocytosis and cell adhesion molecule (CAM) mediated endocytosis. The metabolism and effects of internalized drugs largely depend on the routes of intracellular trafficking, which may lead to degradation in lysosomal compartments, recycling to the plasma membrane or transcytosis to the basal surface of the endothelium.

Table 1 Selected candidate targets for drug delivery to endothelial cells. (EC- endothelial cells, ACE- angiotensin-converting enzyme, TM- thrombomodulin, PECAM- platelet-endothelial adhesion molecule, ICAM- intercellular adhesion molecule, gp- glycoproteins)

Target	Function and Localization	Targeting Advantages	Potential Problems
ACE	Peptidase, converts Ang I to Ang II and cleaves bradykinin. ACE enriched in the lung capillaries.	Selective targeting to lung EC. Intracellular delivery. Vasodilating and anti-inflammatory effects of ACE-inhibition.	Inflammation suppresses targeting. ACE inhibition may be dangerous.
TM	Binds thrombin and converts it into an anticoagulant enzyme.	Intracellular delivery to EC, useful *for* modeling of lung injury in animals.	Inflammation suppresses targeting. Thrombosis due to TM inhibition.

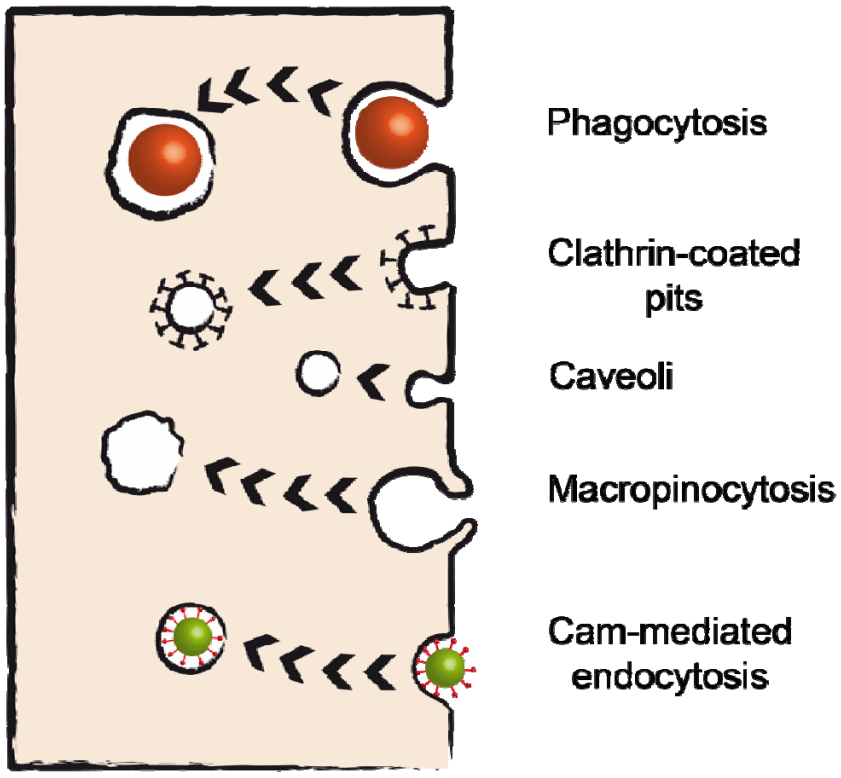

Figure 10 Summary of endocytic pathways.

Another very attractive target for drug delivery are mitochondria, which are membrane-enclosed organelle found in most eukaryotic cells. They can be described as “cellular power plants”, because they generate most of the cells' supply of adenosine triphosphate (ATP), used as the source of chemical energy. In addition, they are involved in a range of other processes such as metabolism, programmed (apoptotic) cell death, Ca^{2+} homeostasis, and cell signaling, control of cell cycle and cell growth.[63] Mutations in mitochondrial DNA are associated with a range of human diseases, again making mitochondria attractive targets for mitochondrial gene therapy.

1.2.5 Polymeric application in drug internalization

During the last decade, intracellular drug delivery has become an emerging area of research in the medical and pharmaceutical field. Many therapeutic agents such as drugs and DNA/oligonucleotides can be delivered not just to the cell but also to a particular compartment of a cell in order to achieve better activity, e.g. proapoptotic drugs to the mitochondria, antibiotics and enzymes to the lysosomes and various anticancer drugs and genes to the nucleus.[64] Therefore, targeting to the appropriate cell is not enough for therapy involving drugs acting intracellularly. Polymeric drug delivery systems can support cellular uptake by pinocytosis (clathrin-coated pits, caveoli, macropinocytosis), adsorptive endocytosis and receptor mediated endocytosis (Figure 10). The uptake of the polymeric systems depends on physicochemical properties i.e. surface charge, size and presence of a specific ligand for the cell surface receptor. Due to smart design of polymeric delivery systems, all these factors can be adopted to specific applications. A protruding function of polymeric carriers is the mediation between the chemical properties of the drug and the internalization pathway. It is known that the plasma membrane is the major obstacle for large and charged molecules. The biological membrane is also responsible for the compartmentalization of cellular organelles and acts as a natural barrier for most molecules. Therefore, the transportation through this barrier is a fundamental requirement for drug delivery systems. There are various factors which are responsible for the rate of diffusion through membranes, such as the size and hydrophobicity of the diffusing molecules.[65] Thus, the biological membrane prevents the entry of hydrophilic molecules. Eukaryotic cells use a number of different endocytotic mechanisms to transport macromolecules and carriers over the plasma membrane barrier (Figure 10). The challenge in the design of drug delivery

systems is therefore to mask the chemical properties of the drug in order to target it inside the cells. Even after the drug has crossed the biological membrane, other problems can occur. Currently, a major challenge is to manipulate or circumvent the non-productive trafficking pathways, such as routing of drugs, proteins and DNA to the lysosomes where they are degraded. Drugs, which are internalized by endocytic pathways and are not stable at endosomal or lysosomal pH, must bypass the endocytic pathway in order to have an efficient activity in the cytosol or at cell organelles.[66]

A novel approach to transfer molecules directly to the cytosol, circumventing the endocytic pathway, is by using cell-penetrating peptides (CPP's). An advantage to use polymeric nanocontainers is that they can be functionalized with cell-penetrating peptides, which mediate the uptake of cargos of different size into cytosol. Cell penetrating peptides have been derived from viral proteins, such as VP22 [67, 68] and HIV-TAT (transactivator of transcription) [69, 70] to novel chemically designed peptides such as poly-arginine.[71, 72] Despite the variability in their origins, these compounds are all capable of crossing biological membranes and carrying the cargo into cells.[73]

TAT and other CPP`s were been shown to deliver cargoes as large as iron nanobeads and fluorescent quantum dots into cells in culture.[74, 75] TAT has also been used to deliver large, active proteins into cells and TAT fusion proteins, to treat cancer, inflammation and other diseases,[76, 77] to deliver phage-encapsulated DNA to cells, and liposome-encapsulated DNA for gene expression in mice.[78, 79] It should also be noted that the efficiency of transduction of TAT and other CPPs depends greatly on the cargo being transduced; this principle is most clearly

demonstrated by difficulties in transducing large, anionic cargo like nucleic acids.[80-83]

The diversity of studied CPP's allows choosing an internalization pathway when designing a drug carrier. Simply altering the oligopeptide by the attachment of molecules changes the internalization pathway depending on the size and hydrophobicity, and therefore affects the efficiency of the delivery system for cytosolic or nuclear targeting.[84, 85] Furthermore, the followed pathway governs the intracellular processing, kinetics and final fate of the CPP and its cargo, and is dependent on several factors including the type of the CPP, type of the attached cargo, the nature of the linkage between the cargo and CPP and the cell system.

2 Oxidative stress and strategies to diminish it

2.1 Oxidative stress

Oxygen, which is essential for the survival of aerobic organisms, can also be harmful to their existence. Oxidative stress is the imbalance between radicals derived from oxygen, and the organism's antioxidant defense mechanism. A “radical” is defined as any atom or biomolecule that contains unpaired electrons. These unpaired electrons influence the chemical reactivity, making the radical more reactive than the corresponding non-radical. The biologically relevant radicals are the superoxide anion ($O_2^{\bullet -}$), the hydroxyl radical ($OH^{\bullet}$) and nitric oxide ($NO^{\bullet}$). Under normal conditions, around 1 to 3 % of the oxygen that is metabolized in the mitochondria is converted to the $O_2^{\bullet -}$ radicals. Some other species are intermediate in the metabolism of O_2 or NO but are not radicals. These intermediate species along with the radical species are called reactive oxygen species (ROS) and reactive nitrogen species (RNS), respectively. The most known example of ROS is hydrogen peroxide (H_2O_2), and of RNS it is peroxynitrite ($ONOO^-$).

The toxic effect of oxidative stress for tissues is based on the reactivity of ROS' with cellular macromolecules, such as proteins, carbohydrates, lipids, and nucleic acids. Exogenous agents like photochemical smog, ozone, pesticides, xenobiotics and ionizing radiation, as well as a variety of endogenous processes, such as mitochondrial respiration, cytochrome P-450 detoxification reactions, phagocytic oxidative bursts, and peroxisomal leakage, can generate significant amount of ROS. ROS have been implicated in aging and [86] various pathological disorders, including cancer, atherosclerosis, rheumatoid arthritis, lupus erythematosus, chronic

inflammatory diseases of the gastrointestinal tract, cataract, diabetes, diabetic retinopathy, Parkinson's disease, Alzheimer's disease.[87-89] In fact, the ability to cope with ROS decreases with age. A wide variety of antioxidant defense systems, enzymatic as well as nonenzymatic, help to prevent and repair ROS-induced damage to tolerable levels. Under ideal circumstances, the rate of production of an oxidatively-modified cellular component should be comparable to that of its removal or repair.

2.2 Natural defense mechanism against oxidative stress

Oxidative stress appears in many pathological conditions, such as inflammation, cancer, aging and organ response to ischemia-reperfusion as a result of modern transplantation techniques or diseases. Although oxidative stress in low concentration has an important role as mediator in normal cellular metabolism and signal transduction, in higher concentrations it can be damaging. Therefore in mammalian cells there exists a complex defense mechanism, which exhibits an antetype for researchers, who try to build artificial defense mechanisms.

Antioxidant substances are defined as substances that significantly delay or prevent oxidation of the substrate when they are present at low concentrations compared to those of oxidizable substrate. The members of the natural antioxidant defense mechanism are mainly small molecular weight substances and enzymes that can convert and detoxify oxidative stress.

The antioxidant defenses include the superoxide dismutase, catalase, gluthatione peroxidase and reductase enzymes, the tripeptide gluthatione, the polypeptide thioredoxine, and peroxidases of the peroxiredoxin family.

As an example, we show the detoxification of $O_2^{\bullet -}$ radicals in the body, via cascade reactions in which SOD, catalase or gluthatione peroxidase are involved. In the first step, SOD catalyses the dismutation of superoxide to hydrogen peroxide and oxygen (Equation 2).

$$2\ O_2^{\bullet -} + 2\ H^+ \rightarrow H_2O_2 + O_2 \qquad \textit{Equation 2}$$

The product of Equation 2, H_2O_2, is a weak oxidant and is relatively stable. In the second step, three main systems can break down H_2O_2: catalase, gluthatione peroxidase and peroxidases of the peroxiredoxin family[3].

Hemoprotein catalase, present in all major body organs, is especially concentrated in the liver. It catalyzes the breakdown of hydrogen peroxide to oxygen and water (Equation 3).

$$2\ H_2O_2 \rightarrow O_2 + 2H_2O \qquad \textit{Equation 3}$$

The second system consists of the gluthatione peroxidase, which removes hydrogen peroxide generated by superoxide dismutase by the oxidation of gluthathione (GSH) to its oxidized form, gluthatione disulphide (GSSG) (Equation 4).

$$2\ GSH + H_2O_2 \rightarrow GSSG + 2H_2O \qquad \textit{Equation 4}$$

GSH is a tripeptide present in millimolar concentration in almost all cells, and represents an important component of the endogenous antioxidant system. Its main function is to act as a co-substrate for gluthatione peroxidases.

The third system consists of peroxidases of the peroxiredoxin family, that reduce hydrogen peroxide to water and alcohol by using reducing equivalents. Thioredoxin is

a polypeptide especially concentrated in the endoplasmatic reticulum, but also found in the mitochondria. In its reduced form it contains two adjacent sulfhydryl groups that are converted to a disulphide in its oxidized form thioredoxin.

Besides various enzymes with protective role, there are various low-molecular-weight molecules that have in vivo antioxidant properties, such as bilirubin, melatonin, lipoic acid, coenzyme Q, uric acid and melamines.[90-93] A large number of dietary constituents exhibit antioxidant effects in vivo, as for example ascorbic acid (vitamin C), or carotenoids. Vitamin C is an important component of the antioxidant system in humans, which acts as a reducing agent, and can therefore scavenge radicals such as $O_2^{\bullet -}$. Carotenoids represent a group of colored pigments widespread in plant tissues and which serve as precursors for vitamin A. As a principal dietary source of vitamin A in humans, they exert an antioxidant action as free radical scavengers.[94]

2.3 Antioxidant therapy

Antioxidant therapy represents an adaptive treatment directed to the down-regulation of excessive oxidative stress. In this respect, several substances, known as members of the natural antioxidant defense mechanism (see 2.2) are applied to reduce the amount of oxidative stress, e.g. catalase or superoxide dismutase. The main problem with proteinogenic antioxidants is their short half-life in the plasma, and the difficulty of protein uptake by the cells. To bypass these difficulties, targeted catalase derivatives were developed by conjugation with carbohydrates. The initial results appear promising.[95]

The rationale behind using SOD is to accelerate the detoxification of the superoxide anion, thus preventing the generation of highly reactive $OH^{\bullet}$ radicals. In vivo studies reported protective effects with SOD treatment,[96, 97] but as its cellular penetration

is poor, this strongly affects and limits its therapeutic potential.[98] Like catalase, the main problem of SOD administration is its short half-life (about 6 min) and the lack of uptake into cells. In most animal studies, protective effects of SOD required multiple or prolonged intravenous infusions of 10-150 mg/kg body weight to reach a therapeutic effect.[99-105] However, the treatment by SOD seems to be a promising alternative to conventional therapies and therefore various attempts were made to improve its biocompatibility.[106, 107] To improve the intracellular availability of SOD, conjugates of SOD were applied, e.g. after PEGylation.[108] Conjugation of proteins with high molecular-weight poly(ethylene glycol) is known to support the uptake of the conjugates into the cell, however the delivery of drugs to sites of increased oxidative stress is needed to increase the efficiency of the artificial antioxidant defense mechanism.

2.3.1 Superoxide dismutase

Copper-zinc superoxide dismutase (CuZnSOD) is a 32 kDa homodimeric protein in the cytoplasm of eukaryotic and bacterial cells that catalyzes the disproportionation of superoxide into oxygen and hydrogen peroxide (Equation 2).[109] Three forms of SOD exist with different subcellular localizations. Those containing copper and zinc are located in the cytosol, [110] while the manganese form is located in the mitochondria, [111] and the extracellular form usually is present outside the plasma membrane and interacting with the matrix components.

In CuZnSOD, each monomer binds one copper and one zinc ion and displays the Greek Key *β*-barrel fold.[112] The enzymatic mechanism proposed for CuZnSOD is the reduction of the oxidized Cu(II) form of the enzyme by superoxide and the release of oxygen (Equation 5).

$O_2^{\bullet-}$ + Cu(II)ZnSOD → O_2 + Cu(I)ZnSOD *Equation 5*

This process is followed by the oxidation of the reduced Cu(I) form by another superoxide anion and two protons, generating hydrogen peroxide (Equation 6).[113-116]

$O_2^{\bullet-}$ + Cu(I)ZnSOD + 2 H^+ → H_2O_2 + Cu(II)ZnSOD Equation 6

The catalytic cycle of CuZnSOD is summarized in Figure 11 and can be described as following. The CuZnSOD molecule is situated in the “resting state” (Figure 11-A), with the copper ion in a distorted square planar conformation. The second step of the cycle can be described as SOD inner sphere transfer state (Figure 11-B). Superoxide is guided to the active site channel by a conserved set of charged amino acid residues. The channel containing these charges narrows from a shallow depression about 24 Å across to a deeper channel about 10 Å wide and finally to a size of less than 4 Å just above the copper ion. An arginine residue at the entrance of the channel helps to attract negatively charged molecules. $O_2^{\bullet-}$ enters the active site channel, displaces a water molecule situated there, and an electron is released after binding to the copper ion. In the third state (Figure 11-C), the histidine bridge breaks, oxygen diffuses out of the active site channel, and a water molecule enters. The copper is now in a trigonal planar conformation characteristic of Cu(I). In the fourth step (Figure 11-D) a second superoxide enters the active site cavity, displaces a water molecule and hydrogen bonds with the second water molecule and a protonated atom of His63. In the final step (Figure 11-E) superoxide accepts an electron from copper and protons from a water molecule and His63 to from hydrogen peroxide. Peroxide diffuses out of the active site and is replaced by a water molecule. The bridge between zinc and copper via His63 is reformed.[117]

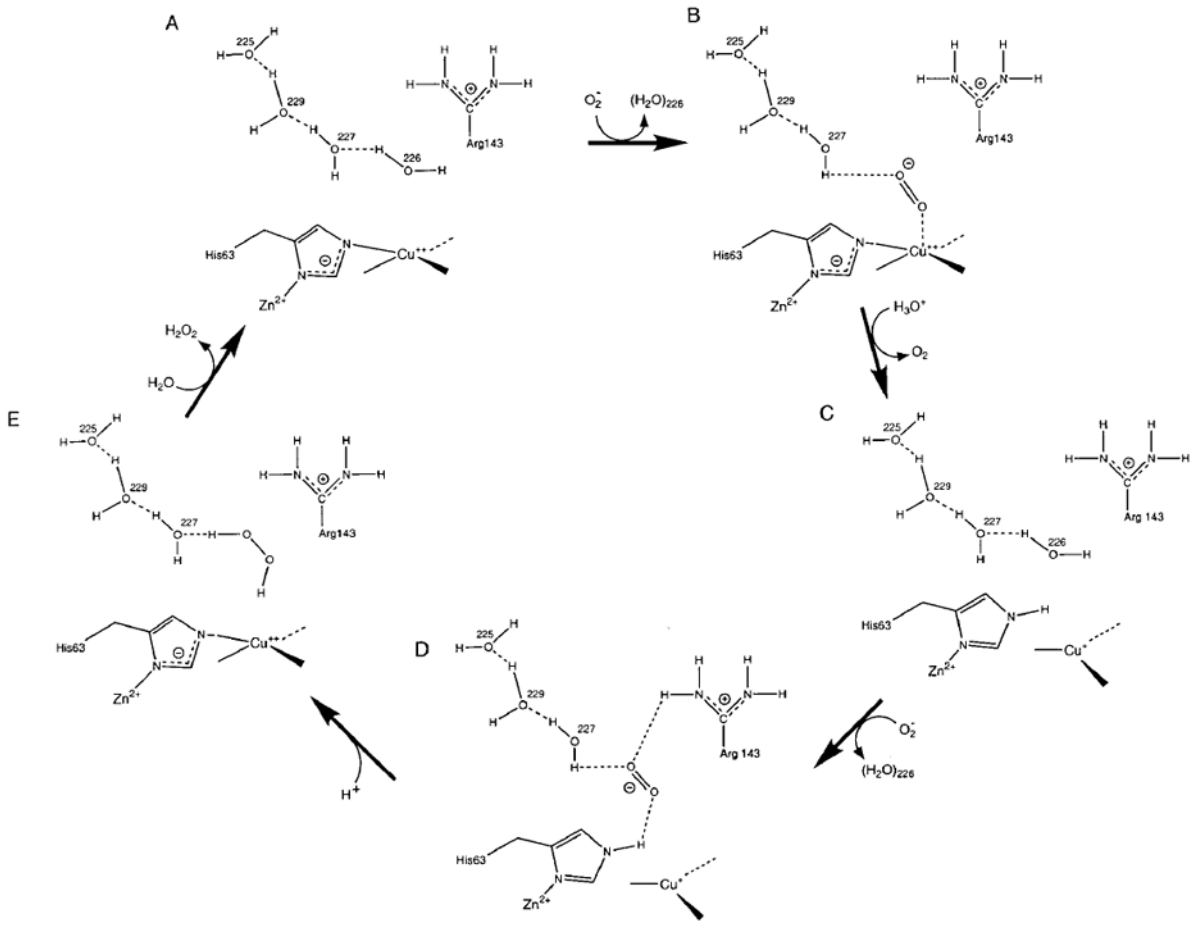

Figure 11 Schematic diagram of the catalytic cycle of CuZnSOD (see paragraph 2.3.1)

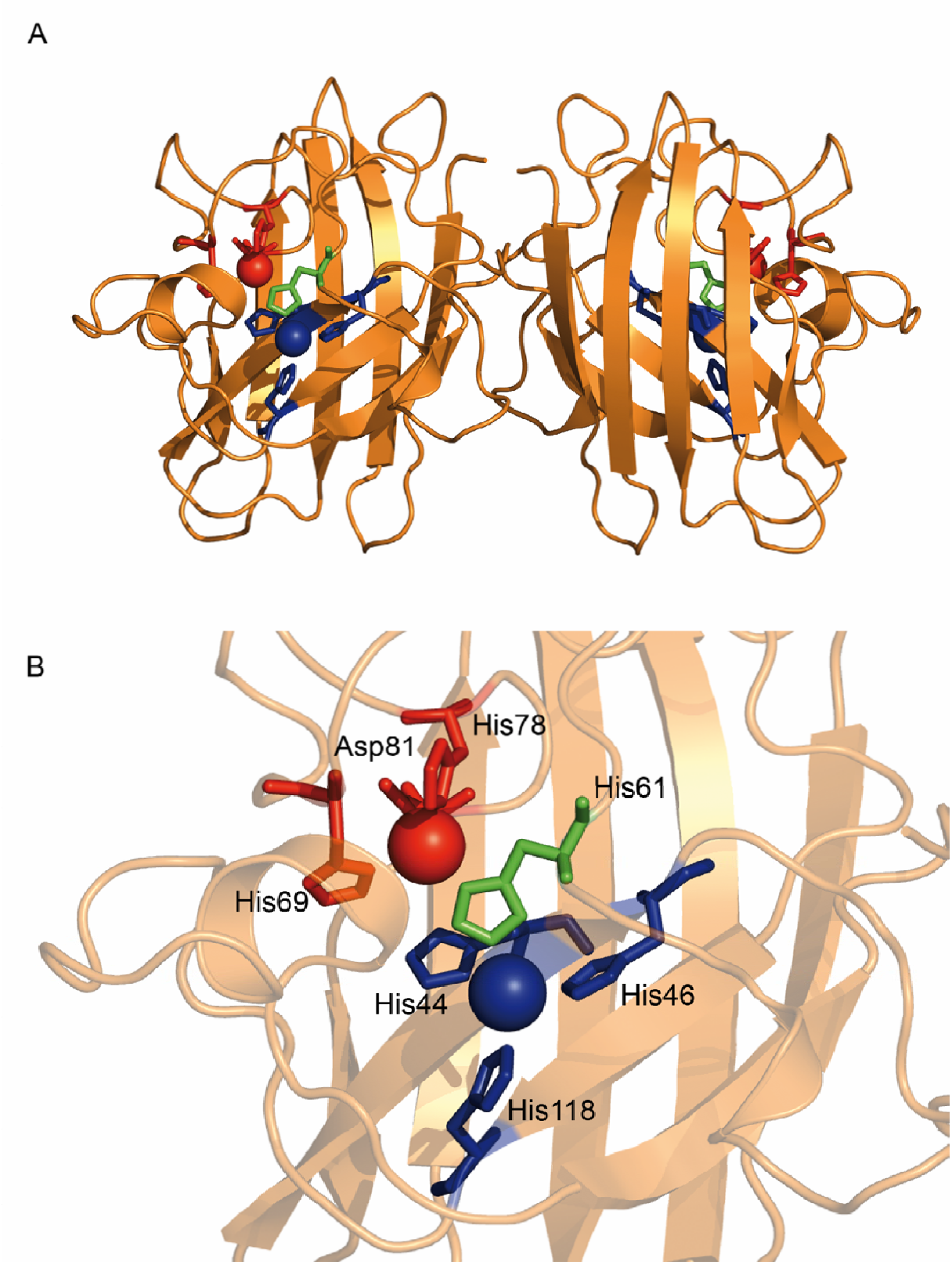

Figure 12 A) Ribbon diagram of reduced homodimeric Cu-Zn SOD (PDB#1SXA) [118].The metal ions are drawn as spheres. B) Enlargement of the SOD active site.

Copper is drawn as blue sphere liganded by His 61, 46, 118, and 44. Zinc is drawn as red sphere liganded by His 78, 61, 69, and Asp 81.

As the active site in CuZnSOD is located in the metal-binding region, several studies were performed to characterize it. Crystallographic and spectroscopic studies showed that the histidine residue 61 (bovine erythrocytes SOD: His63) coordinates the copper and zinc ions (Figure 12). This histidine residue is described as a "histidine bridge", a motif only known in CuZnSOD. The copper binding geometry is described as distorted square planar, as the residues His63, His48, His120 and His46 (bovine erythrocytes SOD: His61, His48, His118, His46) build up this geometric form around the copper ion.

2.4 An antioxidant nanocontainer

In this work we designed an antioxidant nanoreactor based on the encapsulation of CuZnSOD in amphiphilic copolymer nanovesicles (Figure 13). The nanovesicles are formed by self-assembly of amphiphilic copolymer poly-(2-methyloxazoline)-poly-(dimethylsiloxane)-poly-(2-methyloxazoline) (PMOXA-PDMS-PMOXA). We chose this polymer due to its advantages over conventional systems, i.e. liposomes. Polymer nanocontainers can be produced with a controlled mean diameter and low polydispersity compared to liposomes. They were tested and shown to be more stable than liposomes.[1] These represent the main advantages with respect to the application as carriers to improve the drug stability and the circulation life-time. Another factor which could increase dramatically the circulation life-time and therefore the availability of the encapsulated SOD, is the stealth property of the poly-(2-methyloxazoline) chain, comparable to that of PEG. Besides, the polymer used for this study, has an oxygen permeable membrane, as will be shown later. All these

advantages make the nanoreactors a completely new approach of drug delivery systems, in which the cargo is not released, but performs its function within the vesicle.

The nanovesicles, made of poly-(2-methyloxazoline)-poly (dimethylsiloxane)-poly (2-methyloxazoline), successfully encapsulated the SOD protein during their formation by a self-assembling process, as proved by confocal laser-scanning microscopy and fluorescence-correlation spectroscopy. Electron paramagnetic resonance spectroscopy and circular dichroism analyses showed that no structural changes appeared within the proteins once inside the inner cavity of the nanovesicles. The function of this antioxidant nanoreactor was tested by pulse radiolysis which demonstrated that superoxide dismutase remains active inside the nanovesicles. This simple and robust hybrid system provides selective shielding of a sensitive enzyme from proteolytic attack and therefore points to a new direction for developing drug delivery applications.

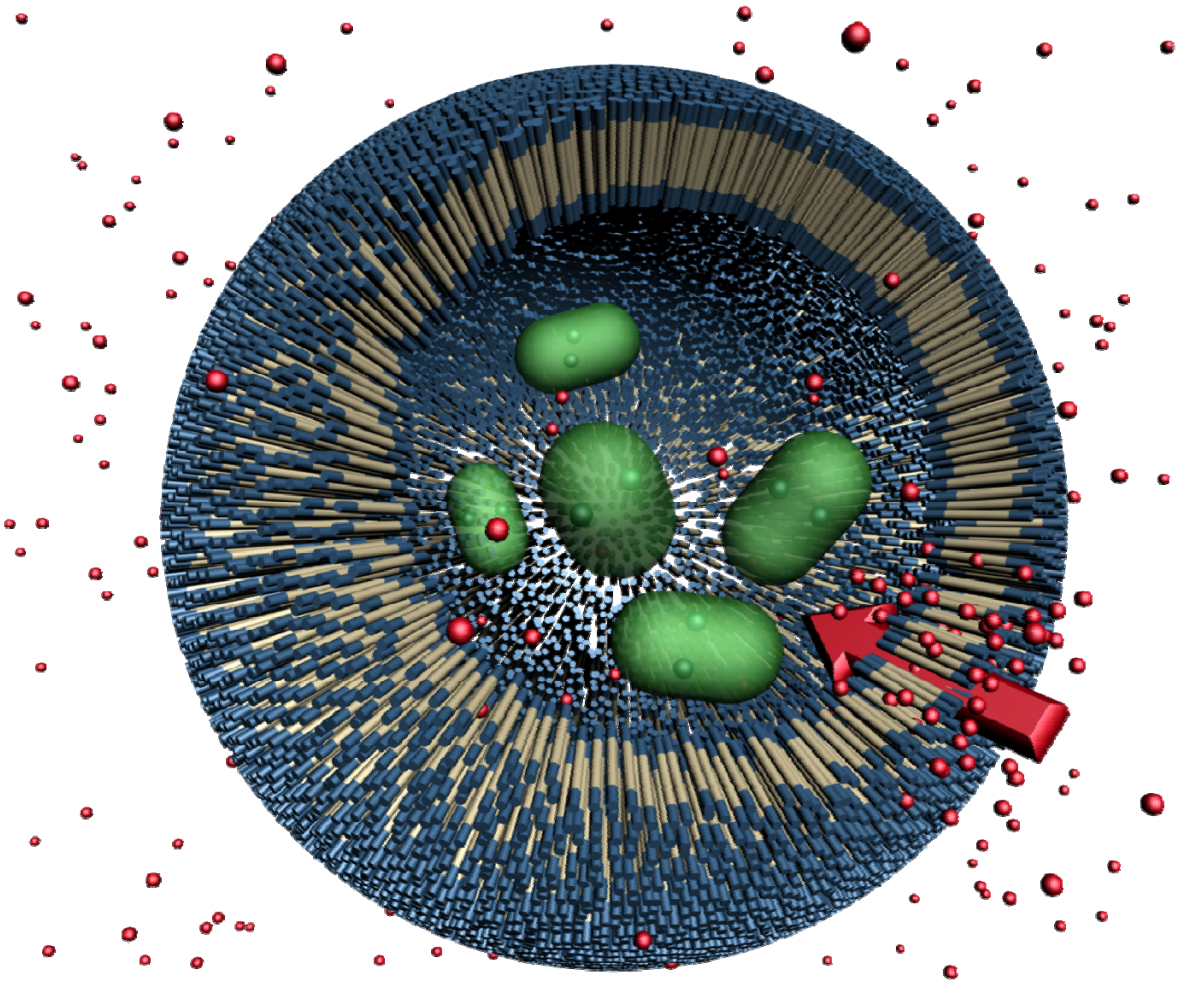

Figure 13 A schematic representation of an antioxidant nanoreactor with encapsulated SOD. The $O_2^{\bullet -}$ is able to penetrate the polymeric shield.

3 Antioxidant nanoreactor based on SOD encapsulation in polymersomes

3.1 The polymersomes – preparation and characterization

3.1.1 Nanocontainer preparation

The synthesis of $PMOXA_n$-$PDMS_m$-$PMOXA_n$ (where n = 15 and m = 110), was described elsewhere.[119] Nanovesicles were prepared according to a modification of a previously published method.[120] Triblock copolymer $PMOXA_{15}$-$PDMS_{110}$-$PMOXA_{15}$ (50 mg) was dissolved in ethanol at 17 % (w/w) and stirred at room temperature for 1 hour. After complete dissolution, this solution was slowly added dropwise to PBS buffer to give a final polymer concentration of 10 mg/ml, and this mixture was stirred overnight at room temperature. The solution was then extruded 20 times through a polycarbonate membrane filter (Millipore) with a well-defined pore size of 200 nm, in order to decrease the size polydispersity of vesicles.[120] Subsequently, the extruded solution was purified by size-exclusion chromatography (SEC) on Sepharose 4B (10 $\times$ 300 mm). The nanostructures were characterized by TEM, SLS, and DLS.

3.1.2 Characterization of polymersomes

Transmission electron microscopy was used to image empty and SOD-containing polymersomes. Nanovesicle dispersions were negatively stained with 2 % uranyl acetate solution and deposited on a carbon-coated copper grid. The samples were examined with a transmission electron microscope (Philips Morgagni 268D) at 293 K.

TEM of self-assembled nanostructures of polymer shows circular objects with radii ranging from 50 to 110 nm, in good agreement with results obtained from cryo-TEM, which indicated nanovesicles with a radius of 117 nm. TEM measurements repeated after long-term storage (> 3 weeks) [119] at 4 °C did not reveal any significant changes, suggesting that the nanovesicles from $PMOXA_{15}$-$PDMS_{110}$-$PMOXA_{15}$ are chemically stable.

Dynamic (DLS) and static (SLS) light-scattering experiments were performed on a ALV (Langen, Germany) goniometer, equipped with an ALV He-Ne laser (λ = 632.8 nm) to determine the sizes and size distribution of empty and SOD-containing polymeric nanovesicles. SOD-encapsulated and empty nanovesicles were prepared by serial dilution to polymer concentrations ranging from 3.33 to 0.1 mg/mL. Light scattering was measured in 10-mm cylindrical quartz cells at angles of 30–150 ° at 293 K. The data for DLS were analyzed using a Williams-Watts function.[121] The size polydispersity of the vesicles was determined according to the literature.[1, 28, 122]

The LS results are presented in Table 2. We calculated a ratio (ρ = R_g/R_H) of the radius of gyration (R_g), obtained from SLS, to the hydrodynamic radius (R_H), from DLS experiments of 0.96, which is characteristic for hollow spherical objects. This so called ρ-parameter is a structure-sensitive property reflecting the radial density distribution of the scattering particle.[123] Based on the assumption of a one-component population, the mean radius of these vesicles is about 150 nm. This larger value, compared to the value obtained from electron microscopy, is due to the fact that in DLS the R_H represents the sum of the particle and its surrounding hydration sphere.

Table 2 Light scattering characterization of empty vesicles

sample	R_g [nm]	R_H [nm]	M [10^8g/mol][a]	A_2 [mol/L/g^2][b]
empty vesicles	150 ± 7	156 ± 8	4.7 ± 0.1	5.1×10^{-11}

[a] M, weight-average molar mass; [b] A_2, second virial coefficient.

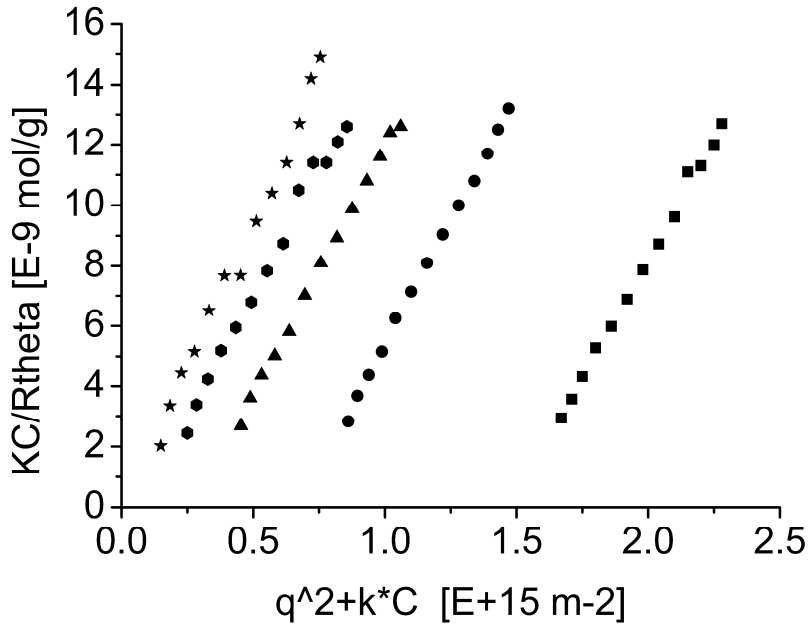

Figure 14 Zimm plot of polymer vesicles without encapsulated SOD.

3.2 SOD Encapsulation: method, efficiency, stability

3.2.1 Fluorescent labeling of SOD

Fluorescently labeled SOD was obtained by reaction of a fluorescent dye, Alexa Fluor 488, with the primary amines of the protein. Labeled SOD was separated from unbound Alexa Fluor 488 by SEC on Sephadex G50 (10 × 300 mm) equilibrated with phosphate-buffered saline (PBS) buffer. The concentration of labeled protein in solution was determined by pulse radiolysis.[124] The number of Alexa Fluor 488/SOD molecules was determined by fluorescence correlation spectroscopy.

3.2.2 Encapsulation of fluorescently labeled SOD in nanovesicles

Encapsulated SOD was obtained by adding the polymer solution as described above to a solution of labeled SOD (0.26 mg/ml) in PBS buffer. The non-encapsulated protein was removed by size exclusion chromatography on a Sepharose 4B column, in PBS buffer eluent. To determine whether the protein can be attacked from the outside of the vesicles, a stock solution of 20 mg/ml of Proteinase K (Roche) was added to the solution of encapsulated, fluorescently labeled SOD at 5 % (v:v), and the mixture was incubated for 4 hours at room temperature.

3.2.3 Characterization of SOD-encapsulating polymersomes

Nanovesicles with encapsulated SOD were characterized by TEM and LS (as described above), and were compared with the empty vesicles. TEM images for SOD-containing nanovesicles (Figure 15) were essentially identical to those for empty vesicles. From SLS and DLS experiments we find a ρ-value of 0.93. The LS characterization of SOD-containing vesicles is presented in Table 3 and Figure 16. Compared to the LS results for empty vesicles (Table 2), SOD containing vesicles show only a minor difference of R_g and R_H. The differences of the values are within the error range.

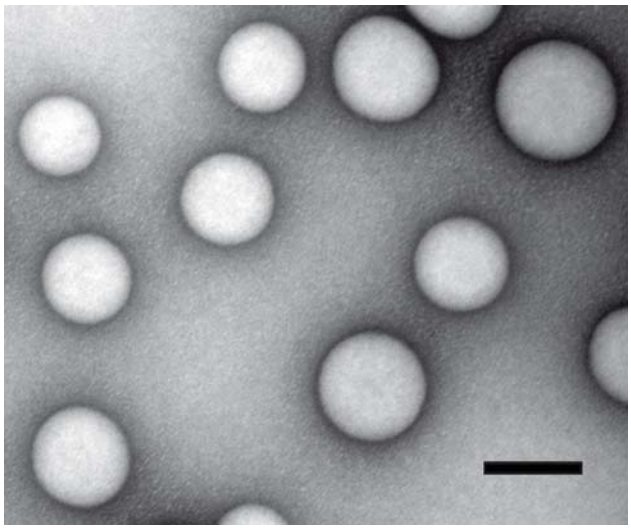

Figure 15 Transmission electron micrograph of SOD-encapsulated in $PMOXA_{15}$-$PDMS_{110}$-$PMOXA_{15}$ vesicles (room temperature; scale bar = 100 nm)

Table 3 Light scattering characterization of SOD-containing vesicles

sample	R_g [nm]	R_H [nm]	M [10^8g/mol][a]	A_2 [mol/L/g^2][b]
SOD-containing vesicles	140 ± 10	149 ± 9	3.4 ± 0.1	1.3×10^{-11}

[a] M, weight-average molar mass; [b] A_2, second virial coefficient.

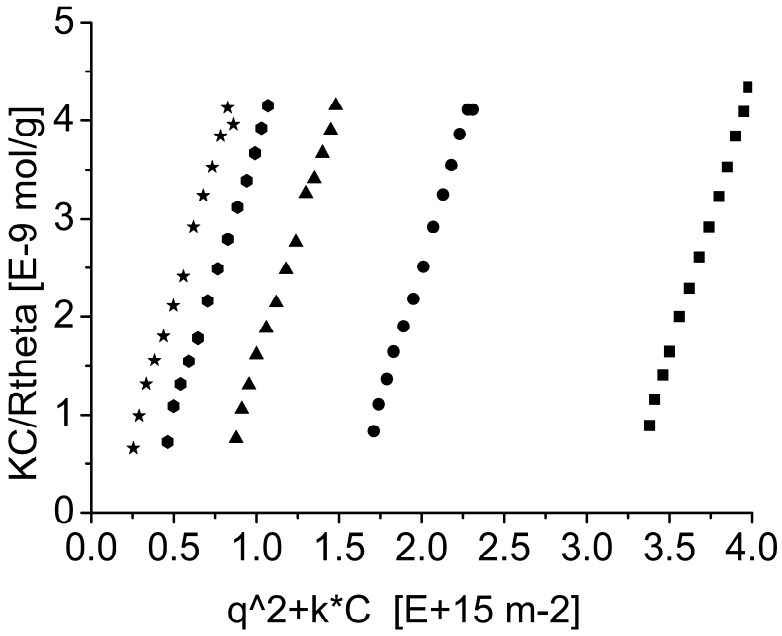

Figure 16 Zimm plot of polymer vesicles with encapsulated SOD.

To check the stability of the nanovesicles containing SOD, they were re-analyzed by LS after 3 weeks of storage at 4 °C; the LS measurements did not indicate any change in radius or size distribution of the nanoreactors over time. This level of stability was expected because of the tightness of the polymer membrane.[1, 125]

All these results indicate that the encapsulation of SOD during the self-assembly process does not influence nanovesicle formation in terms of size or stability.

3.2.4 Laser-Scanning Microscopy/ Fluorescence-Correlation Spectroscopy

To investigate whether the protein is located in the inner space of the nanovesicles, a configuration essential for its shielding, we analyzed nanovesicles prepared with encapsulated SOD, labeled with the fluorescent probe Alexa Fluor 488, by confocal laser scanning microscopy (CLSM) and fluorescence correlation spectroscopy (FCS). Laser scanning microscopy (LSM) and fluorescence correlation spectroscopy (FCS) measurements were performed on a Zeiss LSM 510-META/Confcor2 laser scanning

microscope equipped with an argon laser (488 nm) and a 40× water-immersion objective (Zeiss C/Apochromat 40X, NA 1.2), with the pinhole adjusted to 70 μm. Solutions of polymeric nanoreactors (2–3 mg/ml) with encapsulated SOD-Alexa Fluor 488 were measured at room temperature in special chambered quartz glass holders (Lab-Tek; 8-well, NUNC A/S), which provide optimal conditions for imaging while reducing evaporation of the aqueous solutions. In LSM mode, appropriate filters were chosen and the detector gain, amplifier gain, and offset were adjusted to optimize micrograph quality; images (512 × 512 pixels) were collected with a scan speed of 0.96 s/pixel at 8-bit color depth. In FCS mode, intensity fluctuations were analyzed in terms of the autocorrelation function with the LSM 510/Confocor software package (Zeiss, AG). Spectra were recorded over 30 s, and each measurement was repeated ten times; results are reported as the average of three independent experiments. Adsorption and bleaching effects were reduced by exchanging the sample droplet after 5 minutes of measurement. The excitation power of the Ar laser was P_L = 15 mW, and the excitation transmission at 488 nm was 2 %. To reduce the number of free fitting parameters, the diffusion times for free dye (Alexa Fluor 488) as well as the labeled SOD were independently determined and fixed in the fitting procedure.

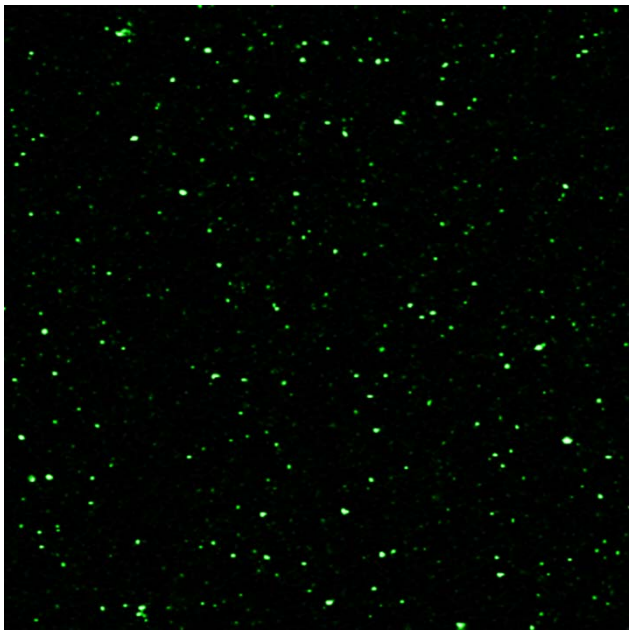

Figure 17 A CLSM micrograph of SOD-Alexa Fluor 488 encapsulated in PMOXA$_{15}$-PDMS$_{110}$-PMOXA$_{15}$ polymeric nanovesicles

We used FCS to examine in more detail the encapsulation of SOD in nanovesicles, by measuring free Alexa 488, non-encapsulated SOD-Alexa Fluor 488, and encapsulated SOD-Alexa Fluor 488. In FCS, a fluctuation correlation approach is applied, in which the laser-induced fluorescence of the excited fluorescent molecules that pass through a very small probe volume is auto-correlated in time to give information about the diffusion times of the molecules. According to the Stokes-Einstein equation, the diffusion times, which are proportional to the R_H of the fluorescent molecules, provide information about interactions of the fluorescent molecules with larger target molecules, including encapsulation of protein in nanovesicles.[122] The results are presented in Figure 18; autocorrelation amplitudes are normalized to 2 to facilitate comparison of diffusion times and the shapes of the curves. The diffusion time (τ_d) for free Alexa Fluor 488 at room temperature is 23 μs (Figure 18, curve a). For non-encapsulated SOD-Alexa Fluor

488, τ_d = 104 μs, which corresponds to R_H = 2.4 nm, in good agreement with the radius of 2.2 nm calculated on the basis of the molecular mass (33 kDa) of SOD-Alexa Fluor 488 (Figure 18, curve b). For encapsulated SOD-Alexa Fluor 488, the multiphasic curve (Figure 18, curve c) indicates the presence of slowly diffusing particles. This population with a reduced diffusion (τ_d = 2.3 ms) represents more than 78 % of the total number of fluorescent particles that pass the confocal volume during the measurement time of 30 s, and corresponds to vesicles that encapsulate SOD-Alexa Fluor 488.

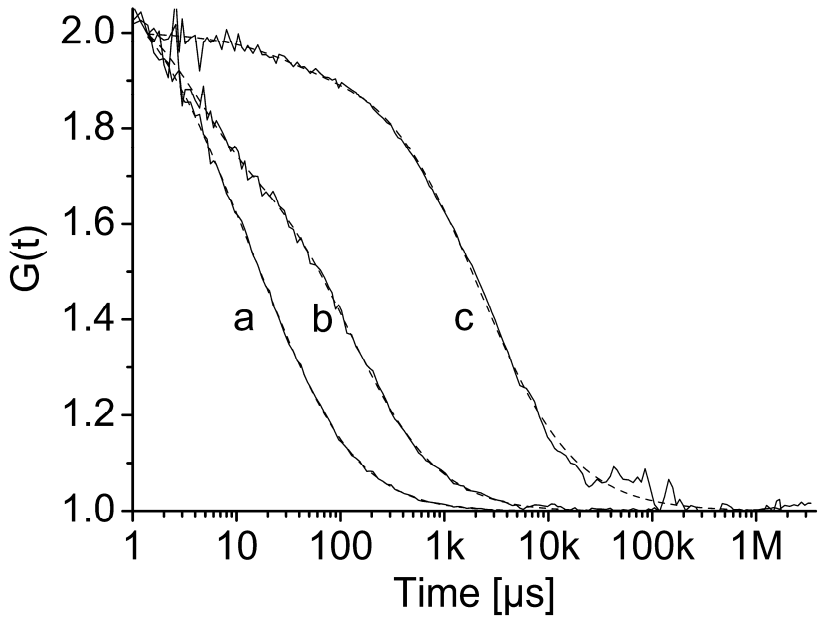

Figure 18 FCS autocorrelation curves. a) Solution of Alexa Fluor 488 (4x10^{-6} mg/ml) in PBS buffer, b) Solution of SOD-Alexa Fluor 488 (6x10^{-6} mg/ml) in PBS buffer, and c) Solution of SOD-Alexa Fluor 488 encapsulated in polymeric nanovesicles from PMOXA$_{15}$-PDMS$_{110}$-PMOXA$_{15}$

FCS measurements were also used to investigate the stability of polymeric nanovesicles encapsulating SOD. After 3 weeks of storage at 4 °C samples were re-analyzed and no release of SOD could be detected.

3.2.5 Estimation of the number of SOD molecules inside the nanovesicles

To estimate the number of SOD molecules encapsulated in the nanovesicles, we compared the molecular brightness, reported as count rates per molecule (cpm, in kHz) of free Alexa Fluor 488, non-encapsulated SOD-Alexa Fluor 488, and encapsulated SOD-Alexa Fluor 488.

We found that one Alexa Fluor 488 is attached to one SOD molecule using a calibration curve of molecular brightness as the function of known concentrations of Alexa Fluor 488 (Figure 19).

SOD-Alexa Fluor 488 in the presence of a polymer environment exhibited less molecular brightness (cpm = 27 kHz) than free Alexa Fluor 488 (cpm = 42 kHz), the difference being mostly attributed to quenching of the dye.[126]

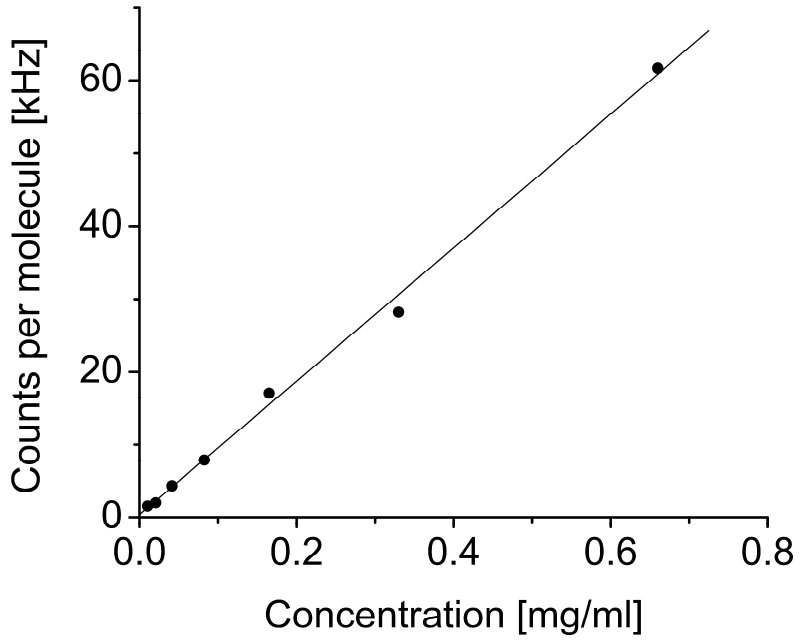

Figure 19 Calibration curve of molecular brightness of free Alexa Fluor 488.

In the case of encapsulated SOD-Alexa Fluor 488, the total molecular brightness (cpm_T) corresponds to the weighted sum of the brightnesses of the individual components (cpm_i) (Equation 7).

$$cpm_T = \sum_{i=1}^{n} a_i \; cpm_i$$ *Equation 7*

cpm_T – total molecular brightness, cpm_i – individual molecular brightness, a_i – proportion of *i* in the total core solution.

By comparing the molecular brightness of the encapsulated SOD-Alexa Fluor 488 solutions with that of the free labeled protein in the presence of polymer, we estimate that an average of 2-5 SOD-Alexa Fluor 488 molecules are encapsulated per nanovesicle when the initial concentration of SOD-Alexa Fluor 488 was 0.1-0.27 mg/ml. This is in agreement with the average number of encapsulated SOD molecules that can be calculated from the initial concentrations of SOD together with the total volume of the inner spaces of the vesicles. The inclusion is a statistical process in which the number of encapsulated molecules is determined by the starting concentrations of the protein. Under the experimental conditions applied, the number of encapsulated SOD molecules is small, as we intended to minimize interactions and functional changes due to confinement in the nanovesicles. In addition, by encapsulating only a small number of SOD molecules we tested the sensitivity of the nanoreactor, a prerequisite for further therapeutic applications. Studies of enzymes at the level of one molecule have the potential to provide significant insight into the detailed spectrum of molecular conformational changes and activities.[127-130]

The block copolymer membranes can be regarded as mimetics of biological membranes, but they are thicker and far more stable than those of the liposomes.[1, 125]

3.3 Selective shielding of SOD from proteolytic attack

As the vesicles are intended to shield SOD from proteolytic attack, we analyzed the FCS data of a solution of encapsulated SOD-Alexa Fluor 488 to which Proteinase K was added in order to see whether the latter can attack the encapsulated enzyme. Proteinase K is commonly used in molecular biology to digest proteins as it is highly active even in the presence of chemicals that denature proteins, such as SDS, urea or EDTA.

The diffusion time of the vesicles that contain labeled SOD did not change when Proteinase K was present, proving that our vesicles protect SOD against enzymatic attack.

In order to investigate whether the encapsulation procedure denatures the protein, we checked for possible geometry changes of the Cu^{II} metal site of the protein by electron paramagnetic resonance (EPR), and characterized the protein's backbone structure by circular dichroism (CD).

3.3.1 Application of electron paramagnetic resonance for determination of the Cu site of SOD structure determination

To characterize structural information of paramagnetic materials such as some transition metals and free radicals, the EPR-spectroscopy is the preferred method. While for crystals the x-ray crystallography is the best method for structure determination, the EPR-spectroscopy can provide structure informations about paramagnetic molecules without any limitation concerning their physical state (single crystals, solutions, powders, frozen solution, gases), where the resolution of x-ray diffraction is limited to a few Å. And the position of protons is not clearly resolved which further decreases the resolution of the x-ray technique. In this respect, EPR-

spectroscopy has also a wide application in detection of biological processes, because the samples were measurable under physiological-like conditions. In order to simulate an EPR spectrum we have to take into account the interactions that are relevant for the paramagnetic species: (1) Gyromagnetic tensor which represents the interaction of the unpaired electron characterising the paramagnetic molecule and the external magnetic field. (2) Hyperfine interaction tensor which represents the interaction between the magnetic momentum of the unpaired electron and the magnetic momentum associated with the nuclei which form the first coordination sphere around the metal (in our case, copper).

By introducing as input relevant values for the gyromagnetic and hyperfine tensors, according to the overall shape of the spectrum we obtain by using a simulation program (such as Simfonia, Bruker), a simulated spectrum as a first order simulation. With these values, a finer simulation is possible with optimising the parameters, until the best fit is obtained. This represents an iterative procedure that can be achieved using Minuit Simplex procedure. As soon as a reasonable simulation was obtained, the extracted values, especially the g-factor and the principal hyperfine constants, were used for structure model. Structure determination is based on comparison of known values for certain geometries of the first order coordination sphere around the metal to the ones obtained from the spectrum simulation, to predict possible structures of the unknown structures.

3.3.1.1 Theory

EPR is a technique which records a resonant absorption of a microwave radiation by a paramagnetic ion located in a static magnetic field. To understand this phenomenon, knowledge about paramagnetism, the energy-levels in a system with

permanent magnetic field and the principle, how to detect these transitions among the energy-levels is required.

3.3.1.2 Paramagnetism

Paramagnetism is observed in atoms, molecules and lattice-defects with an odd number of electrons or for free atoms and ions with partially filled inner shells. The magnetic moments of these atoms are weak and they have a low interaction among each other. They are randomly ordered, if no magnetic field is applied. When they are placed in a magnetic field, they will align parallel to the magnetic field, and an overall magnetization of the sample can be put into evidence. The alignment depends on the strength of the magnetic field.

3.3.1.3 Zeeman-effect

An electron has an intrinsic kinetic momentum which is called electron spin $\vec{s}$,and this one can be associated with a magnetic field produced by its angular motion. So an electron has an magnetic moment $\vec{\mu}$. The explanation of the Zeeman-effect can be simply understand using a two-level system. The interaction between a magnetic field B_0 and an unpaired electron with a magnetic moment $\vec{\mu}$ is known as the Zeeman-effect. Two energy-levels are possible: A lower energy level is reached, when the magnetic moment $\vec{\mu}$ is aligned with the magnetic field (s = $-\frac{1}{2}$) and an upper energy-level is obtained for a magnetic moment which is aligned against the magnetic field (s = $+\frac{1}{2}$). The energy corresponding to each orientation of the spin is the product of μ and B_0, where the magnetic moment μ is defined as,

$$\mu = -g_e \cdot \mu_B \cdot s$$ *Equation 8*

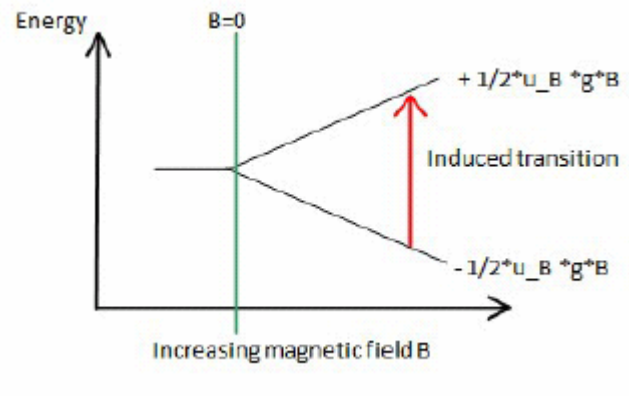

Figure 20 Energy diagramm of possible states (spin up or down).

where the definition of the Bohr magneton $\frac{e \cdot h}{2 \cdot m_e} = \mu_B$ is. Because the spin s can be up or down, the possible energy levels are:

$$E = \pm \frac{1}{2} \cdot g_e \cdot \mu_B \cdot B_0$$ *Equation 9*

The total energy-difference between the two levels is:

$$U = \vec{\mu} \cdot \vec{B}$$ *Equation 10*

g is the electronic splitting factor (g-factor for free electrons: g_e = 2:0023192778). The energy levels are shown in Figure 20. An absorption in a magnetic field takes place when the energy of the frequency $h \cdot \upsilon$ is the same as the energy-difference U of the two states, and this represents the resonance condition. The EPR spectra are obtained as first derivative of a normal absorption spectrum, for better resolution. The spectrum is obtained experimentally by variation of the external magnetic field, once the sample is placed in this field, simultaneously with the microwave irradiation of the sample. When the magnetic field induce a difference of the energy levels that is

equal to the microwave energy of irradiation, the resonance takes place and absorption can be seen. The signal is the first derivative $\left(\frac{\delta\, amplitude}{\delta\, magnetic\ field} \right)$.

If we look at an electron which belongs to a molecule, its own magnetic moment will be changed due the interaction with the nuclei which has a magnetic momentum different to zero, such as N, P, Cl, etc. This represents the hyperfine interaction, and can be used to characterise the first order coordination sphere around the metal, or the structure of the free radical where the unpaired electron is delocalised.

The formula to obtain the effective gyromagnetic value of an isotropic spectrum is given in Equation 11. The resulting energy $h \cdot \upsilon$ is equal to the energy difference in Equation 10:

$$g = 714.4775 \cdot \frac{\upsilon}{B_0} \qquad \textit{Equation 11}$$

where υ is in Ghz and B_0 is in Gaussian units.

3.3.1.4 Principal shapes of spectra

The EPR can distinguish between different symmetries of the matrix in which the molecules can be arranged, in a referential that can be connected to the molecular frame. In this way the EPR spectrum analysis can give informations about the local symmetry in a single crystal and provide structural informations, exactly as X-ray diffraction. Therefore, a principal axis system exists for each paramagnetic molecule with the principal g-factors, g_x; g_y; g_z, for each axis. In this way the molecular frame is characterised by the anisotropy of the gyromagnetic tensor. The shape of a spectrum directly corresponds to the absorptions along each principal axis. Different principal g-factors are shown in Figure 21.

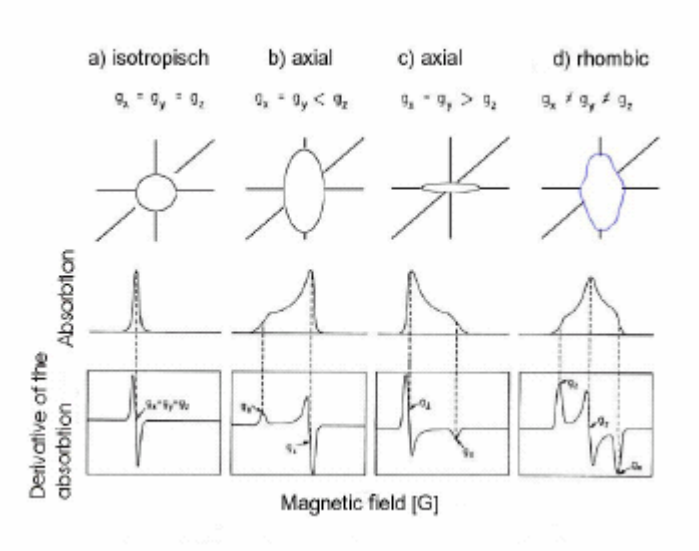

Figure 21 The principle g-factors determine the shape of a spectrum. a) isotropic, b) axial, c) axial, d) rhombic.

3.3.1.5 Hyperfine splitting

A more complicated splitting is reached as a result of hyperfine interactions. The principle is the fact, that a bar magnets can be influenced by another bar magnet. The distance of the two bar magnet determines the strength of interaction. Therefore, the nuclear spin I is involved and Equation 10 becomes $A \cdot s \cdot I$. A is the principal hyperfine constant. The nuclear spin of copper is $\frac{3}{2}$ for example. This leads to four absorptions, because the electronic states were split in four nuclear sub-levels between $-I...(-I+1)...I$ for all allowed magnetic quantum numbers M_I. The hyperfine interaction can be regarded exactly as the gyromagnetic tensor, and in this respect its symmetry (isotropic, axial, rhombic) can give more details for the geometry of the coordination sphere around the metal, and the nature of the first order ligand nuclei.

3.3.2 Integrity of the metal site of incorporated SOD

In CuZn-SOD, Cu^{II} is located at the enzyme active site, where it plays a role in the disproportionation of $O_2^{\bullet -}$ to dioxygen and hydrogen peroxide at near diffusion-controlled rates.[131]

It is possible to characterize the first coordination sphere around the metal ion by EPR, both from the point of view of geometry and identification of nuclei with non-zero spin, as the values of the spin Hamiltonian parameters can be related to the various distortions of the copper environment.

Electron paramagnetic resonance (EPR) spectra of the solutions of incorporated SOD in nanocontainers were recorded at 77 K with a CW Bruker ElexSys500 X-band CW spectrometer, equipped with a helium temperature control system (ER4112HV), to which the wave-guide resonance cavity was attached. Microwave power was adjusted at levels below the saturation condition (2 mW for high field measurements and 10 mW for low field measurements). The modulation frequency was 100 kHz and the modulation amplitude was 0.5 mT; other spectral parameters were adjusted for each spectrum individually. Multiple spectra (150) were acquired to optimize the signal-to-noise ratio, and 3rd-order polynomial averaging was used for subsequent noise reduction. The spectral parameters were obtained with the SIMFONIA software package (Bruker Instruments Inc., Manning Park, Billerica, MA), where co-axial g and hyperfine tensors were assumed. Gaussian line shapes were considered with the line-width adjusted for each spectrum. All spectral simulations assumed natural abundance ratios of Cu isotopes. The *g*-values were referenced to diphenylpicryhydrazyl (DPPH) (g = 2.0036) as an external standard.

In Figure 22, the curve a) shows the EPR spectrum of a frozen-solution of the encapsulated protein, obtained after a multiple acquisition (more than 500 spectra) procedure. The simulation is obtained with a third-order perturbation theory approach (Figure 22, curve b) provides the values of the gyromagnetic and hyperfine tensors: $g_{\perp}$ = 2.067, $g_{||}$ = 2.263; $A_{\perp}$ = 4.1 mT, $A_{||}$ = 13.9 mT. These values, which are similar to those previously obtained for frozen solutions of bovine CuZn-SOD,[132] indicate that the metal site is not affected by the encapsulation procedure. The metal-binding site of the oxidized form of wild-type CuZn-SOD, has been characterized by X-ray diffraction, EPR and electronic spectroscopy and shows the Cu^{II} ion to be five-coordinate, with four histidyl side chains in a tetrahedrally distorted arrangement and one axially located water molecule.[131, 133] Unfortunately, the multiple acquisition procedure required for the encapsulated enzyme impedes the use of either D2-EPR or pulse-EPR methods that would provide more information on the fine details of the coordination sphere of copper.[134].

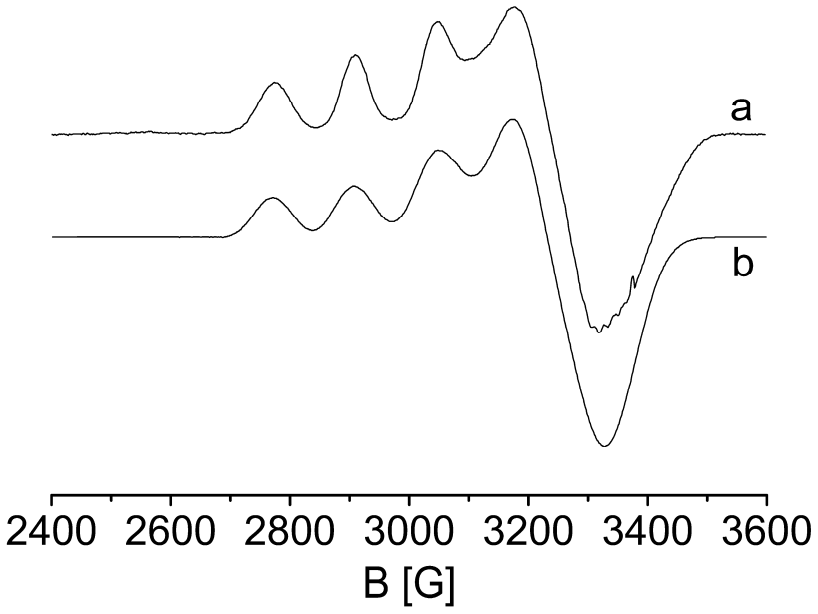

Figure 22 EPR spectra. a) CuZn-SOD encapsulated in nanovesicles of triblock copolymer $PMOXA_{15}$-$PDMS_{110}$-$PMOXA_{15}$, at 77 K b) Simulation obtained from a third-order perturbation theory approach.

3.3.3 Circular dichroism

In order to study if the backbone of SOD was modified by encapsulation, circular dichroism (CD) spectra (180–260 nm) were recorded to determine the impact of the labeling and encapsulation conditions on the SOD molecule. Circular dichroism is a form of spectroscopy based on the differential absorption of left- and right handed circularly polarized light. Structural motifs in proteins, such as helices and sheets, are CD spectral signatures and can be therefore used for structural identification.

Measurements were made with an Applied Photophysics Chirascan CD spectrometer. Encapsulated SOD-Alexa Fluor 488 collected from the SEC purification step was centrifuged with a filter device (Centricon YM-10, Millipore, 10 kDa nominal molecular weight cutoff) at 5000 g to exchange the PBS buffer with MilliQ water (18 MΩ cm; Purelab UHQ, Elga) and compared with unlabeled SOD solubilized in MilliQ water.

The CD spectra of SOD-Alexa Fluor 488 before and after the encapsulation procedure (Figure 23) differ only in signal intensity, which is due to sample concentrations. This indicates that if the encapsulation caused any changes to the protein backbone, these changes were reversible.[135]

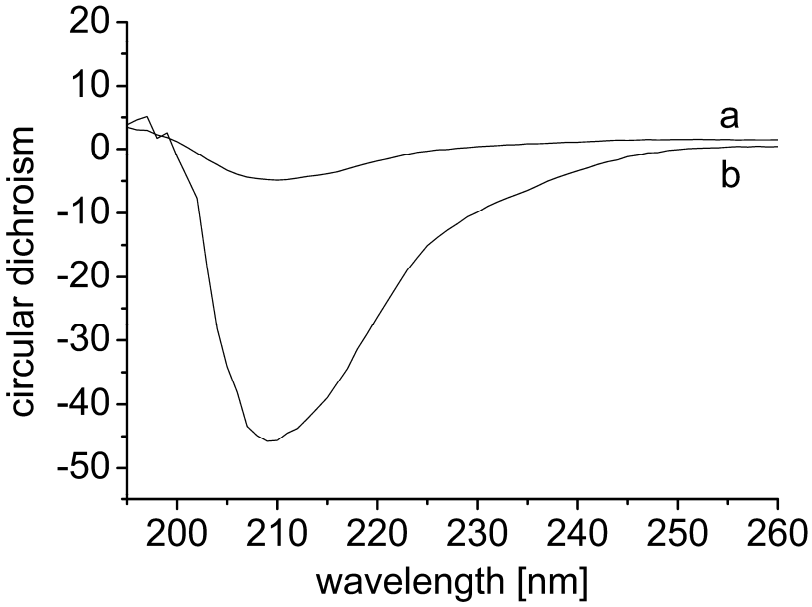

Figure 23 CD Spectra. a) SOD-Alexa Fluor 488 separated from SOD-filled nanovesicles by SEC. b) SOD-Alexa Fluor 488 not exposed to the encapsulation conditions.

3.4 Quantification of the anti-inflammatory capacity of encapsulated SOD

3.4.1 Pulse radiolysis as a method to determine the SOD activity

The activity of SOD in the polymeric nanovesicles was investigated by pulse radiolysis with a Febetron 705 (Titan Systems Corp., San Leandro, CA, USA) 2.3-MeV accelerator with a pulse width (fwhm) of <50 ns as the radiation source; the optical system consists of a 75-W Xe arc lamp (Hamamatsu, Schüpfen, Switzerland), a 1- or 2-cm-optical-path quartz cell (Hellma GmbH and Co. KG, Müllheim, Germany), and an Acton SP300i monochromator (Roper Scientific, Ottobrunn, Germany). For signal detection of kinetic traces, a R928 photomultiplier (Hamamatsu) with a DHPCA-200 amplifier (Femto Messtechnik GmbH, Berlin,

Germany) with a DL7100 digital storage oscilloscope (Yokogawa Electric Corporation, Tokyo, Japan) is used; a Princeton Instruments PI-MAX 512T gateable ICCD camera (Roper Scientific) is used for detection of time-resolved spectra. $O_2^{\bullet -}$ is formed by irradiation of oxygenated sodium formate (1 M) solutions at pH 8.5. SOD activity is calculated from rates of decay of $O_2^{\bullet -}$, measured at 280 nm, in the presence and absence of SOD. Doses between 10 and 50 Gy/pulse were applied. When experiments with vesicles are carried out, extensive light scattering is observed, which results in a lower signal amplitude. The 100 Hz ripple is caused by the electronic equipment.

3.4.2 SOD activity assay of nanocontainers encapsulating SOD

We performed pulse radiolysis measurements on series of free and encapsulated SOD samples to determine whether encapsulated SOD remains active. CuZn-SOD is active across a wide pH range (5.0–9.5) and under various environmental conditions,[124, 136, 137] thus, we hypothesized that the protein's function would not be affected by the encapsulation procedure. Our hypothesis was supported by observations that encapsulated SOD remains structurally intact. We have previously succeeded in encapsulating other proteins in nanovesicles, for example, β-lactamase and the purine-specific nucleoside hydrolase of *Trypanosoma ViVax* (TvNH), and found that activity was preserved.[23, 138]

In pulse radiolysis, the kinetics of the superoxide anions dismutation is measured directly; the method is sensitive (10 nM), accurate, and reproducible. Figure 24-1 shows the rate of dismutation of the superoxide anion in the presence of empty nanovesicles (curve a, $t_{½} \approx 300$ ms) compared to SOD-filled nanovesicles (curve b, $t_{½} \approx 4$ ms). The very rapid dismutation of superoxide anions in the presence of

encapsulated SOD, together with the finding that SOD is present only in the inner space of the nanovesicles, demonstrates that the nanovesicles are permeable to superoxide and $HO_2^{\bullet}$, and may be described as nanoreactors. The *in situ* activity assays together with structural characterization of the protein establish that no changes to the protein occur during the encapsulation procedure. The reaction rate of the encapsulated enzyme is similar to that of the free enzyme (Figure 24), which indicates that the diffusion of $O_2^{\bullet -}$ through the triblock copolymer wall is not rate-limiting.

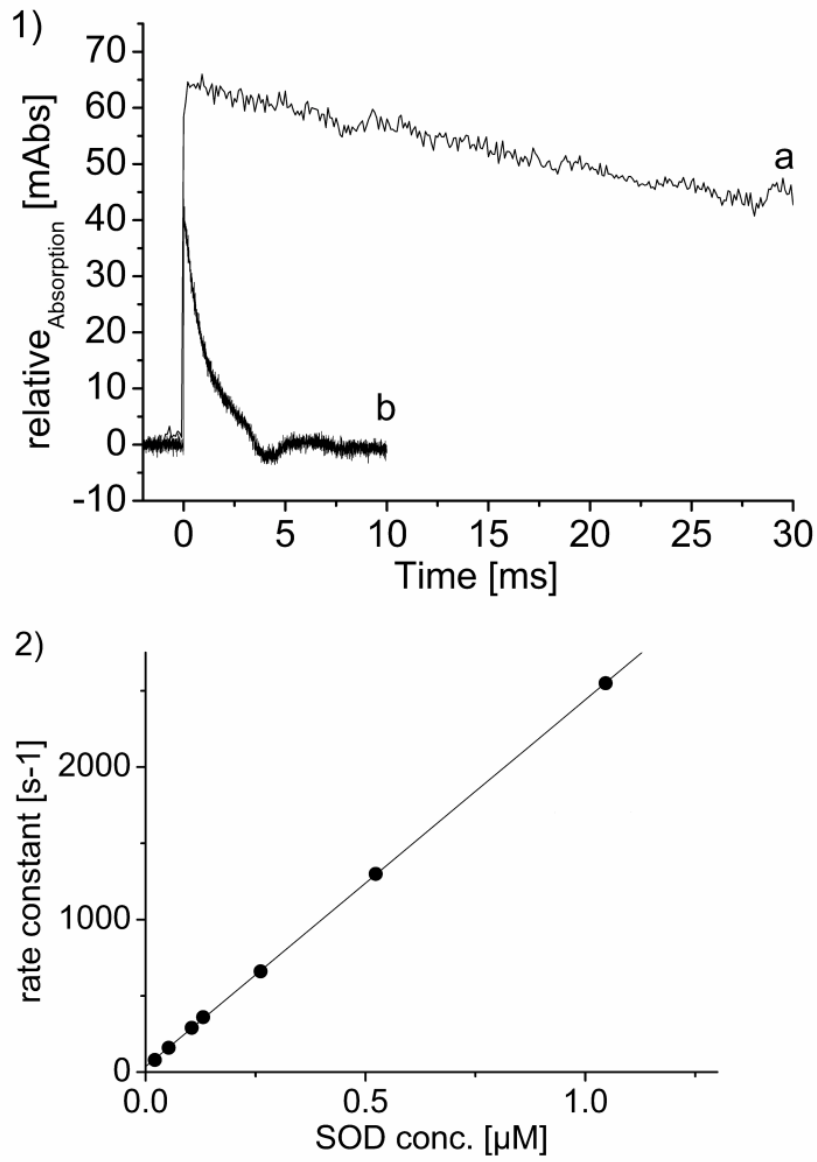

Figure 24 1) Pulse radiolysis assay. 1a) Uncatalyzed decay observed at 280 nm of 80 μM superoxide produced by a 50 ns pulse of an aerated solution of 1.0 M formate and 10 mM phosphate, pH 8. 1b) Superoxide decay catalyzed by SOD (ca. 0.12 μM) encapsulated in $PMOXA_{15}$-$PDMS_{110}$-$PMOXA_{15}$ vesicles (10 mg polymer). 2) Pulse radiolysis standard curve for different concentrations of SOD.

We constructed a calibration curve from a series of pulse-radiolysis determinations of the activity of free SOD in solution (Figure 24-2) and, assuming free diffusion of superoxide, used the curve to calculate the amount of SOD encapsulated. By taking into account the number of nanovesicles formed in the solution of 10 mg/ml of polymer with a weight average molar mass M = 3.4×10^8 g/mol (determined from LS experiments) and the concentration of encapsulated SOD (determined by pulse radiolysis), the average encapsulation number is 10 protein molecules/nanovesicle (for an initial concentration of SOD of 0.3 mg/ml). This value is slightly higher than the maximum average number of encapsulated SOD-Alexa Fluor 488 molecules obtained from molecular brightness measurements, where only labeled-SOD molecules are counted (non-labeled protein molecules are invisible). We emphasize that within the experimental errors and inherent limitations of each method, the results of these two independent methods are in good agreement. Due to the small number of encapsulated SOD molecules the intermolecular interactions or conformational changes due to confinement of SOD in the nanovesicles can be considered negligible. Because of the mild encapsulation that occurs during the self-assembly process of nanovesicle formation, as well as the experimental conditions aimed at restricting the number of enzyme molecules encapsulated, SOD remains

fully active and the dismutation of superoxide takes place in the inner space of the nanoreactor.

According to studies on the permeability of bilayer lipid membranes to superoxide radicals, the transport of $O_2^{\bullet -}$ is strongly dependent on the structural state of the membrane and on the localization of the substrate; the permeability coefficient estimated at 2.1×10^{-6} – 7.6×10^{-8} cm/s in lipids.[139, 140] Generally, for lipid bilayers, channels for anion transport must be incorporated, and the bilayers tend to break down and release encapsulated compounds over time. However, the polymeric nanoreactors described here are permeable to both dioxygen and superoxide and do not require anion channels.[4, 23, 141, 142] As the protein acts inside the polymer vesicles, our nanoreactor is inherently simpler and overcomes the problems connected to efficient release in the body, which are common to conventional carriers, such as liposomes and other polymeric nanocontainers. The antioxidant nanoreactor is not limited to use with superoxide dismutase, it can be chemically modified for specific targeting approaches and enables the simultaneous encapsulation of other proteins to extend its applicability.

4 A Total antioxidant nanoreactor

4.1 The Concept and goal of the co-encapsulation

As described in paragraphs 2.2 (Equation 2) and 2.3.1 (Equation 5, Equation 6), SOD converts superoxide anions to hydrogen peroxide and dioxygen as the part of a natural antioxidant defense mechanism. Hydrogen peroxide itself is weak, and compared to the half-life of $O_2^{\bullet -}$, quite stable. Therefore it needs to be degraded to achieve a sufficient antioxidant effect of the antioxidant nanoreactors *in vivo*. In order to obtain a total antioxidant nanoreactor we propose to co-encapsulate SOD and horseradish peroxidase (HRP). These two enzymes would act together in a cascade reaction and fully convert $O_2^{\bullet -}$ via hydrogen peroxide to water and dioxygen.

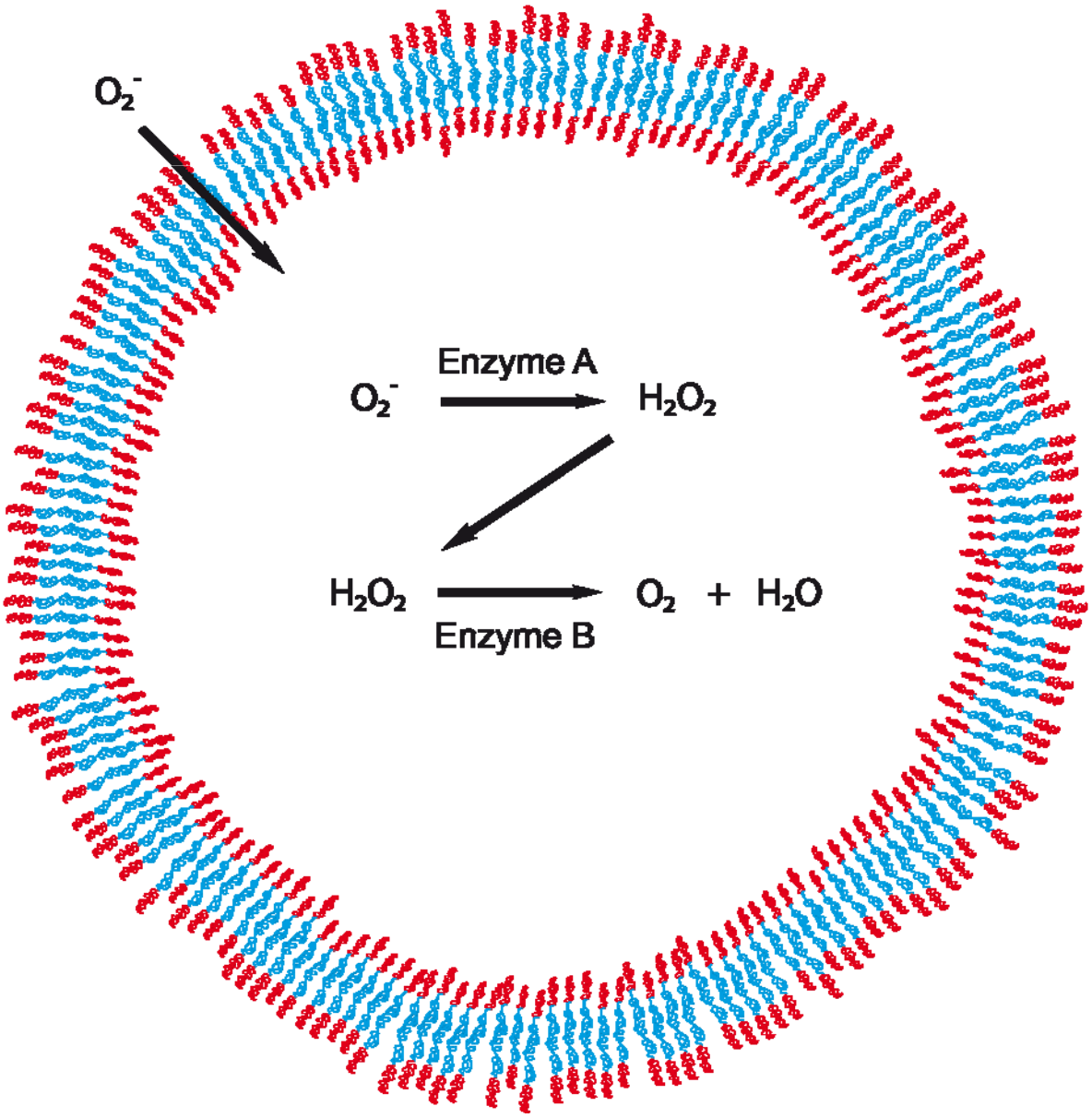

Figure 25 A schematic drawing of the concept and mechanism of the coencapsulation of an enzymatic cascade detoxifying $O_2^{\bullet-}$.

Firstly, catalase was chosen as the second enzyme, in order to be co-encapsulated with SOD. Preliminary tests to establish the experimental methods to track catalase inside vesicles showed that neither hydrogen peroxide as reactant, nor water or dioxygen as products, offer the possibility of spectrophotometric detection at very low concentrations which predominate inside the nanoreactor. Therefore horseradish

peroxidase (HRP), as a second enzyme to enable a cascade reaction towards a complete detoxification of superoxide radicals. HRP is a heme-containing enzyme of 40 kDa, which catalyses the reduction of hydrogen peroxide to water. In the presence of specific substrates, which act as hydrogen donors, HRP can oxidize these substrates by using hydrogen peroxide. We chose the fluorescent dye Amplex Red (AmpR) for tracking hydrogen peroxide degradation. In the presence of HRP, the AmpR reacts in a 1:1 stoichiometry with hydrogen peroxide to produce highly fluorescent resorufin (Figure 26). This way the use of AmpR allows to detect if the co-encapsulated enzymes work sequentially to detoxify $O_2^{\bullet -}$ in water and dioxygen.

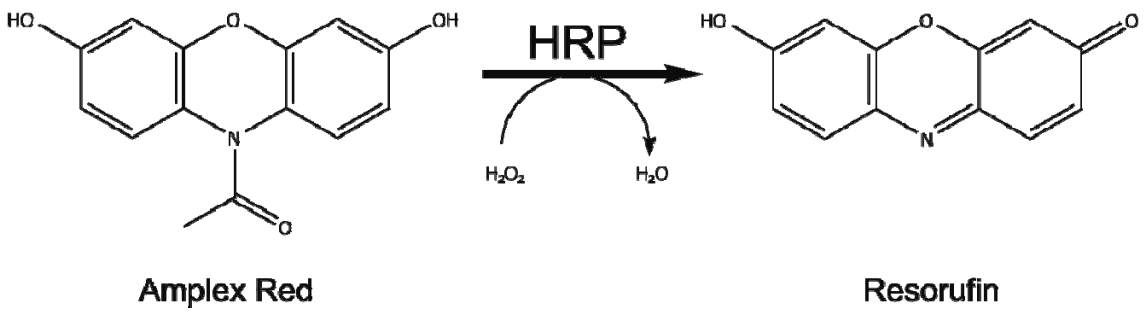

Figure 26 Reaction of AmpR to resorufin, catalyzed by the enzyme HRP

4.2 Preliminary results on SOD-HRP co-encapsulation

The co-encapsulation was accomplished like the encapsulation of SOD described in paragraph 3.2.2. The following concentrations of the enzymes and fluorescent dye were used: SOD (0.5 mg/ml), HRP (0.2 mg/ml) and AmpR (0.012 mg/ml). The nanocontainers with co-encapsulated SOD, HRP and AmpR were purified as described above (paragraph 3.2.2).

A xanthine/ xanthine oxidase reaction was used to generate superoxide anions. Xanthine oxidase is found in mammal liver and is responsible for the catalysis of

hypoxanthine to xanthine oxidation (Equation 12), and can further catalyze the oxidation of xanthine to uric acid and superoxide (Equation 13).

Equation 12

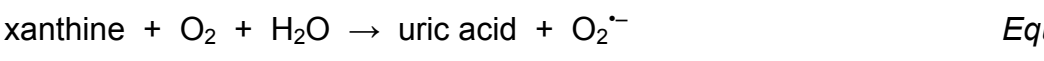

Equation 13

Several control experiments were accomplished:

a. The reliability of the superoxide anion production was proved by measuring the kinetics of the reaction, following the appearance of uric acid at 290 nm (Figure 27). The concept of the cascade reaction of SOD, HRP and AmpR was proved by adding them together in a reaction vessel without encapsulation (Figure 28-a). The concentrations of the reactants were similar to those in the encapsulation experiment, described above.

To prove if xanthine oxidase or the product of its reaction with xanthine can oxidize AmpR, they were mixed together. Figure 28-b shows clearly, that xanthine oxidase or its product does not react with AmpR.

The purified nanocontainers, xanthine (0.15 mM, pH 7.5) and xanthine oxidase (0.5 u/mL, 50 mM potassium phosphate buffer, pH 7.5) were mixed in a ratio of 1:1:1 (v:v:v). The kinetics of the reaction was measured by fluorescence spectroscopy using a luminescence spectrometer LS55 (Perkin Elmer) and analysis software FL Winlab (Perkin Elmer). The mixture was excited at 530 nm and the emission of the sample was measured at 580 nm. Figure 28 shows that the cascade reaction of SOD, HRP and AmpR worked properly.

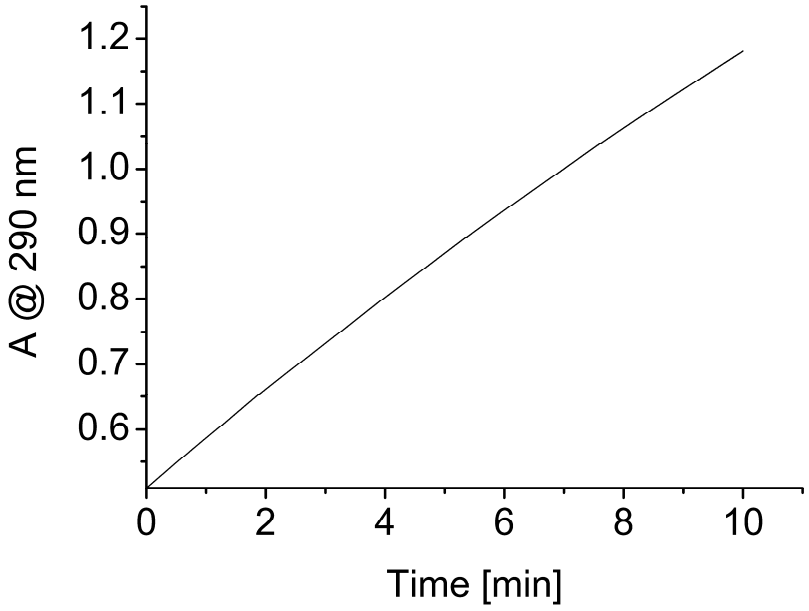

Figure 27 Kinetics of the appearance of uric acid, produced by xanthine/ xanthine oxidase.

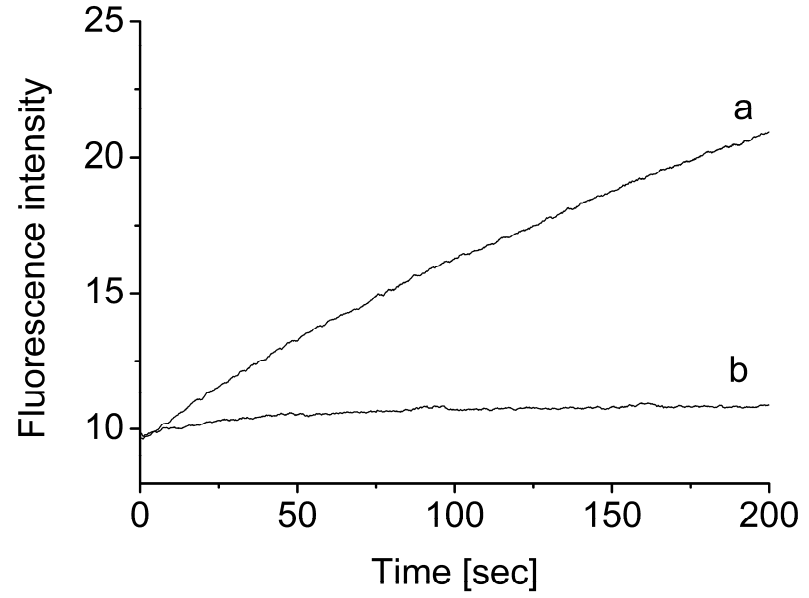

Figure 28 a) Kinetics of the reaction of SOD, HRP and AmpR (not encapsulated). Superoxide was generated using xanthine/ xanthine oxidase. b) Kinetics of the reaction of AmpR with xanthine/ xanthine oxidase. Both measurements were accomplished at λ_{ex}: 530 nm, λ_{em}: 580 nm.

Preliminary tests showed, that $O_2^{\bullet -}$, generated by xanthine/ xanthine oxidase is able to cause a reaction in the presence of nanocontainers, although the received change in the fluorescence signal is close to the detection limit of the used luminescence spectrometer (Figure 29). Figure 29 shows that after an initial decrease of the fluorescence signal a clear increase appears which is related to the conversion of AmpR to resurofin by HRP. A reason for this low yield in fluorescence intensity can be the autooxidation of amplex red and its low amount encapsulated in the nanocontainers. Further experiments are planned to improve the conditions to establish and characterize the cascade reaction in situ in vesicles and test the efficiency of the complete antioxidant nanoreactors.

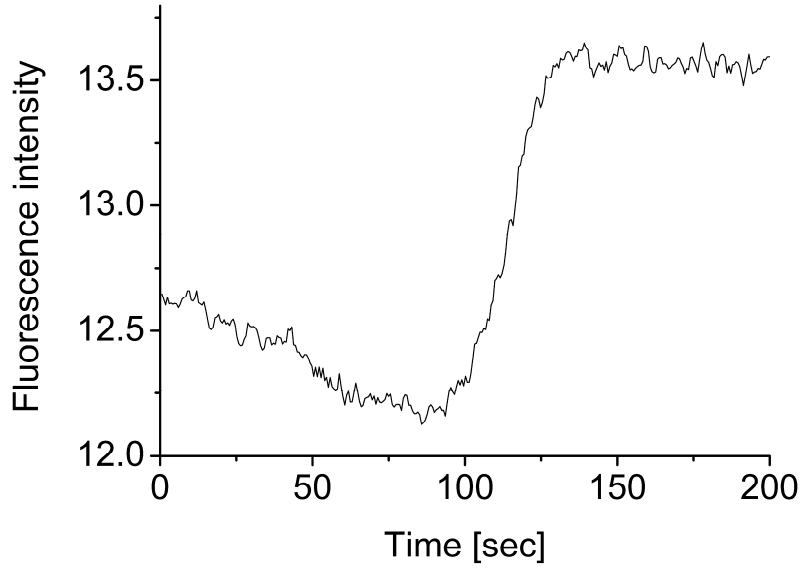

Figure 29 Kinetics of the conversion of AmpR to Resurofin encapsulated in nanocontainer with coencapsulated SOD, HRP, AmpR after addition of xanthine/ xanthine oxidase. Measurement was accomplished at λ_{ex}: 530 nm, λ_{em}: 580 nm.

5 Materials for encapsulation of SOD, HRP, AmpR in nanocontainers

5.1 Shielding of SOD by encapsulation in polymeric nanocontainer

CuZn-SOD from bovine erythrocytes (Sigma Aldrich), Alexa Fluor® 488 (Invitrogen), dimethylsulfoxide (DMSO; Aldrich), Sephadex G-50 (Fluka), uranyl acetate (Sigma Aldrich), and ethanol (99.8 %; Fluka) were used without any further treatment. Sepharose 4B (Sigma Aldrich) and polycarbonate membrane filters (Millipore, 200 nm) were used. Alexa Fluor 488 (Invitrogen) was used as described in the manufacturer's protocol (MP00143, http://www.invitrogen.com). Proteinase K (Roche) was used as described in the manufacturer's protocol.

5.2 Co-encapsulation of SOD, HRP, AmpR

CuZn-SOD from bovine erythrocytes (Sigma Aldrich), HRP from horseradish (Sigma), dimethylsulfoxide (DMSO; Aldrich), potassium phosphate (Sigma), Sephadex G-50 (Fluka), and ethanol (99.8 %; Fluka) were used without any further treatment. Sepharose 4B (Sigma Aldrich) and polycarbonate membrane filters (Millipore, 200 nm) were used. Amplex Red (Invitrogen) was used as described in the manufacturer's protocol (http://www.invitrogen.com). Xanthine/ xanthine oxidase (Sigma) was used as described in the manufacturers protocol (X1875).

6 Conclusions

We designed and tested novel antioxidant nanoreactors based on encapsulation of SOD in superoxide radical-permeable nanovesicles. This represents the first example of an antioxidant nanoreactor which overcomes the problems linked to conventional drug delivery systems. SOD encapsulated in block copolymer nanovesicles formed via self-assembly, is located in the inner cavity of the nanovesicles, and the mild encapsulation process does not affect the structural or functional integrity of the enzyme. The polymeric membrane of the nanovesicles is capable of both protecting the encapsulated SOD and allowing penetration by $O_2^{\bullet -}$, where the conversion to hydrogen peroxide and oxygen is catalyzed. Compared with conventional drug nanocarriers made of liposomes or polymers, our system combines the advantages of a polymer shield with an *in situ* active protein. The tight polymeric membrane of the nanovesicles prevents release of the encapsulated protein from the nanoreactor.[119] The sensitivity of this nanoreactor is high, as proved by the observation that SOD activity was measured although the number of encapsulated SOD molecules is small. The production of nanoreactors is straightforward, involving simple self-assembly of the amphiphilic copolymer in the presence of the protein. The level of superoxide permeability obviates the necessity of inserting artificial channels in the polymer membrane, as usually done with nanoreactors.[4, 23, 141, 142] The antioxidant nanoreactors remain stable over several weeks of storage at 4 °C. Selective permeability of the polymeric membrane may be generally useful to improve the bioavailability of proteinaceous pharmaceuticals. The association of the second enzyme inside the nanoreactor,

which can convert hydrogen peroxide to water, represents a step further to obtain a complete antioxidant nanoreactor. Preliminary tests were performed to study the conditions specific for the cascade reaction involving SOD and HRP together. Further experiments are planned to improve the system of the cascade reaction in situ in vesicles and test the efficiency of the complete antioxidant nanoreactor.

7 References

1. Nardin, C., M. Winterhalter, and W. Meier, *Giant Free-Standing ABA Triblock Copolymer Membranes.* Langmuir, 2000. **16**(20): p. 7708-7712.
2. Soo, P.L. and A. Eisenberg, *Preparation of block copolymer vesicles in solution.* Journal of Polymer Science, Part B: Polymer Physics, 2004. **42**(6): p. 923-938.
3. Yu, K. and A. Eisenberg, *Bilayer Morphologies of Self-Assembled Crew-Cut Aggregates of Amphiphilic PS-b-PEO Diblock Copolymers in Solution.* Macromolecules, 1998. **31**(11): p. 3509-3518.
4. Vriezema, D.M., et al., *Self-Assembled Nanoreactors.* Chemical Reviews, 2005. **105**(4): p. 1445-1489.
5. Alexandridis, P., *Amphiphilic copolymers and their applications.* Current Opinion in Colloid & Interface Science, 1996. **1**(4): p. 490-501.
6. Antonietti, M. and S. Foerster, *Vesicles and liposomes: A self-assembly principle beyond lipids.* Advanced Materials, 2003. **15**(16): p. 1323-1333.
7. Zhang, L. and A. Eisenberg, *Multiple morphologies of "crew-cut" aggregates of polystyrene-b-poly(acrylic acid) block copolymers.* Science (Washington, D. C.), 1995. **268**(5218): p. 1728-31.
8. Discher, B.M., et al., *Polymersomes: Tough vesicles made from diblock copolymers.* Science, 1999. **284**(5417): p. 1143-1146.
9. Tuzar, Z. and P. Kratochvil, *Micelles of block and graft copolymers in solutions.* Surface and Colloid Science, 1993. **15**: p. 1-83.
10. Price, C., *Colloidal properties of block copolymers.* Developments in Block Copolymers, 1982. **1**: p. 39-80.
11. De Gennes, P.G., *Macromolecules and liquid crystals: reflections on certain lines of research.* Solid State Physics, Supplement, 1978. **14**: p. 1-18.
12. Gao, Z., et al., *Block Copolymer "Crew-Cut" Micelles in Water.* Macromolecules, 1994. **27**(26): p. 7923-7.
13. Halperin, A., M. Tirrell, and T.P. Lodge, *Tethered chains in polymer microstructures.* Advances in Polymer Science, 1992. **100**(Macromol.: Synth., Order Adv. Prop.): p. 31-71.
14. Cornelissen, J.J.L.M., et al., *Helical superstructures from charged poly(styrene)-poly(isocyanodipeptide) block copolymers.* Science, 1998. **280**(5368): p. 1427-1430.
15. Kimura, S., et al., *Vesicular Self-Assembly of a Helical Peptide in Water.* Langmuir, 1999. **15**(13): p. 4461-4463.
16. Kukula, H., et al., *The Formation of Polymer Vesicles or "Peptosomes" by Polybutadiene-block-poly(L-glutamate)s in Dilute Aqueous Solution.* Journal of the American Chemical Society, 2002. **124**(8): p. 1658-1663.
17. Forster, S. and T. Plantenberg, *From self-organizing polymers to nanohybrid and biomaterials.* Angewandte Chemie, International Edition, 2002. **41**(5): p. 688-714.
18. Broz, P., et al., *Cell targeting by a generic receptor-targeted polymer nanocontainer platform.* Journal of controlled release, 2005. **102**(2): p. 475-88.

19. Christian, N.A., et al., *Tat-Functionalized Near-Infrared Emissive Polymersomes for Dendritic Cell Labeling.* Bioconjugate Chemistry, 2007. **18**(1): p. 31-40.
20. Sauer, M. and W. Meier, *Polymer nanocontainers with controlled permeability.* Australian Journal of Chemistry, 2001. **54**(3): p. 149-151.
21. Sauer, M., D. Streich, and W. Meier, *pH-sensitive nanocontainers.* Advanced Materials (Weinheim, Germany), 2001. **13**(21): p. 1649-1651.
22. Monnard, P.A., *Liposome-entrapped Polymerases as Models for Microscale/Nanoscale Bioreactors.* Journal of Membrane Biology, 2003. **191**(2): p. 87-97.
23. Nardin, C., et al., *Nanoreactors based on (polymerized) ABA-triblock copolymer vesicles.* Chemical Communications, 2000(15): p. 1433-1434.
24. Graff, A., et al., *Virus-assisted loading of polymer nanocontainer.* Proceedings of the National Academy of Sciences of the United States of America, 2002. **99**(8): p. 5064-5068.
25. Schurtenberger, P., et al., *Preparation of monodisperse vesicles with variable size by dilution of mixed micellar solutions of bile salt and phosphatidylcholine.* Biochimica et Biophysica Acta, Biomembranes, 1984. **775**(1): p. 111-14.
26. Philippot, J.R., S. Mutaftschiev, and J.P. Liautard, *Extemporaneous preparation of large unilamellar liposomes.* Biochim Biophys Acta FIELD Full Journal Title:Biochimica et biophysica acta, 1985. **821**(1): p. 79-84.
27. Van Zanten, J.H. and H.G. Monbouquette, *Characterization of vesicles by classical light scattering.* Journal of Colloid and Interface Science, 1991. **146**(2): p. 330-6.
28. Van Zanten, J.H., *Characterization of vesicles and vesicular dispersions via scattering techniques.* Surfactant Science Series, 1996. **62**(Vesicles): p. 239-294.
29. Vasey, P.A., et al., *Phase I clinical and pharmacokinetic study of PK1 [N-(2-hydroxypropyl)methacrylamide copolymer doxorubicin]: First member of a new class of chemotherapeutic agents-drug-polymer conjugates.* Clinical Cancer Research, 1999. **5**(1): p. 83-94.
30. Saifer, M.G.P., R. Somack, and L.D. Williams, *Plasma clearance and immunologic properties of long-acting superoxide dismutase prepared using 35,000 to 120,000 dalton poly-ethylene glycol.* Advances in Experimental Medicine and Biology, 1994. **366**(Free Radicals in Diagnostic Medicine): p. 377-87.
31. Abuchowski, A., et al., *Effect of covalent attachment of polyethylene glycol on immunogenicity and circulating life of bovine liver catalase.* Journal of Biological Chemistry, 1977. **252**(11): p. 3582-6.
32. Maksimenko, A.V., *Experimental antioxidant biotherapy for protection of the vascular wall by modified forms of superoxide dismutase and catalase.* Current pharmaceutical design, 2005. **11**(16): p. 2007-16.
33. Storm, G. and M.C. Woodle, *Long circulating liposome therapeutics: from concept to clinical reality.* Long Circulating Liposomes, 1998: p. 3-16.
34. Viau, A.T., et al., *Safety evaluation of free radical scavengers PEG-catalase and PEG-superoxide dismutase.* Journal of Free Radicals in Biology & Medicine, 1986. **2**(4): p. 283-8.

35. Kotze, A.F., et al., *Chitosan and chitosan derivatives as absorption enhancers for peptide drugs across mucosal epithelia.* Drugs and the Pharmaceutical Sciences, 1999. **98**(Bioadhesive Drug Delivery Systems): p. 341-386.
36. Henriksen, I., G. Smistad, and J. Karlsen, *Interactions between liposomes and chitosan.* International Journal of Pharmaceutics, 1994. **101**(3): p. 227-36.
37. Takeuchi, H., et al., *Enteral absorption of insulin in rats from mucoadhesive chitosan-coated liposomes.* Pharmaceutical Research, 1996. **13**(6): p. 896-901.
38. Wang, J., D. Mongayt, and V.P. Torchilin, *Polymeric micelles for delivery of poorly soluble drugs: Preparation and anticancer activity in vitro of paclitaxel incorporated into mixed micelles based on poly(ethylene glycol)-lipid conjugate and positively charged lipids.* Journal of Drug Targeting, 2005. **13**(1): p. 73-80.
39. Dziubla, T.D., A. Karim, and V.R.K. Muzykantov, *Polymer nanocarriers protecting active enzyme cargo against proteolysis.* Journal of Controlled Release, 2005. **102**(2): p. 427-439.
40. Harada, A. and K. Kataoka, *Supramolecular assemblies of block copolymers in aqueous media as nanocontainers relevant to biological applications.* Progress in Polymer Science, 2006. **31**(11): p. 949-982.
41. Hsiue, G.-H., et al., *Environmental-sensitive micelles based on poly(2-ethyl-2-oxazoline)-b-poly(L-lactide) diblock copolymer for application in drug delivery.* International Journal of Pharmaceutics, 2006. **317**(1): p. 69-75.
42. Liu, S.-Q., et al., *Bio-functional micelles self-assembled from a folate-conjugated block copolymer for targeted intracellular delivery of anticancer drugs.* Biomaterials, 2007. **28**(7): p. 1423-1433.
43. Lukyanov, A.N., et al., *Polyethylene Glycol-Diacyllipid Micelles Demonstrate Increased Accumulation in Subcutaneous Tumors in Mice.* Pharmaceutical Research, 2002. **19**(10): p. 1424-1429.
44. Mu, L., T.A. Elbayoumi, and V.P. Torchilin, *Mixed micelles made of poly(ethylene glycol)-phosphatidylethanolamine conjugate and D-a-tocopheryl polyethylene glycol 1000 succinate as pharmaceutical nanocarriers for camptothecin.* International Journal of Pharmaceutics, 2005. **306**(1-2): p. 142-149.
45. Gregoriadis, G. and A.T. Florence, *Liposomes in drug delivery. Clinical, diagnostic and ophthalmic potential.* Drugs, 1993. **45**(1): p. 15-28.
46. Corvo, M.L., et al., *Liposomal formulations of Cu,Zn-superoxide dismutase: physico-chemical characterization and activity assessment in an inflammation model.* Journal of Controlled Release, 1997. **43**(1): p. 1-8.
47. Aoki, H., et al., *High-efficiency entrapment of superoxide dismutase into cationic liposomes containing synthetic aminoglycolipid.* Chemical & Pharmaceutical Bulletin, 1997. **45**(8): p. 1327-1331.
48. Miyajima, K., et al., *Effects of cholesterol on the miscibility of synthetic glucosamine diesters in lipid bilayers and the entrapment of superoxide dismutase into the positively charged liposomes.* Chemical & Pharmaceutical Bulletin, 1993. **41**(11): p. 1889-94.
49. Regnault, C., et al., *Effect of encapsulation on the anti-inflammatory properties of superoxide dismutase after oral administration.* Clinica Chimica Acta, 1995. **240**(2): p. 117-27.

50. Dokka, S., et al., *Oxygen radical-mediated pulmonary toxicity induced by some cationic liposomes.* Pharmaceutical Research, 2000. **17**(5): p. 521-525.
51. Aramaki, Y., et al., *Induction of apoptosis in WEHI 231 cells by cationic liposomes.* Pharmaceutical Research, 2000. **17**(5): p. 515-520.
52. Barenholz, Y., *Liposome application: problems and prospects.* Current Opinion in Colloid & Interface Science, 2001. **6**(1): p. 66-77.
53. Huang, C., *Studies on phosphatidylcholine vesicles. Formation and physical characteristics.* Biochemistry FIELD Full Journal Title:Biochemistry, 1969. **8**(1): p. 344-52.
54. Fonseca, M.J., M.A. Alsina, and F. Reig, *Coating liposomes with collagen (Mr 50,000) increases uptake into liver.* Biochim Biophys Acta FIELD Full Journal Title:Biochimica et biophysica acta, 1996. **1279**(2): p. 259-65.
55. Fidler, I.J., et al., *Design of liposomes to improve delivery of macrophage-augmenting agents to alveolar macrophages.* Cancer Research, 1980. **40**(12): p. 4460-6.
56. Hammer, D.A. and D.E. Discher, *Synthetic cells - self-assembling polymer membranes and bioadhesive colloids.* Annual Review of Materials Research, 2001. **31**: p. 387-404.
57. Lee, J.C.M., et al., *Preparation, stability, and in vitro performance of vesicles made with diblock copolymers.* Biotechnology and Bioengineering, 2001. **73**(2): p. 135-145.
58. Palivan, C.G., et al., *Responsive self-assembled nanostructures.* Nanotechnology in Biology and Medicine, 2007: p. 32/1-32/26.
59. Walde, P. and S. Ichikawa, *Enzymes inside lipid vesicles: preparation, reactivity and applications.* Biomolecular Engineering, 2001. **18**(4): p. 143-177.
60. Li, Y.-Y., et al., *Novel Stimuli-Responsive Micelle Self-Assembled from Y-Shaped P(UA-Y-NIPAAm) Copolymer for Drug Delivery.* Biomacromolecules, 2006. **7**(11): p. 2956-2960.
61. Chilkoti, A., M.R. Dreher, and D.E. Meyer, *Design of thermally responsive, recombinant polypeptide carriers for targeted drug delivery.* Advanced Drug Delivery Reviews, 2002. **54**(8): p. 1093-1111.
62. Lin, J.J., et al., *Adhesion of Antibody-Functionalized Polymersomes.* Langmuir, 2006. **22**(9): p. 3975-3979.
63. McBride, H.M., M. Neuspiel, and S. Wasiak, *Mitochondria: More Than Just a Powerhouse.* Current Biology, 2006. **16**(14): p. R551-R560.
64. Rawat, A., et al., *Targeted intracellular delivery of therapeutics: an overview.* Pharmazie, 2007. **62**(9): p. 643-658.
65. Belting, M., S. Sandgren, and A. Wittrup, *Nuclear delivery of macromolecules: barriers and carriers.* Advanced Drug Delivery Reviews, 2005. **57**(4): p. 505-527.
66. Gupta, B., T.S. Levchenko, and V.P. Torchilin, *Intracellular delivery of large molecules and small particles by cell-penetrating proteins and peptides.* Advanced Drug Delivery Reviews, 2005. **57**(4): p. 637-651.
67. Murphy, A.L. and S.J. Murphy, *Catch VP22: the hitch-hiker's ride to gene therapy?* Gene therapy, 1999. **6**(1): p. 4-5.
68. Sciortino, M.T., et al., *Of the three tegument proteins that package mRNA in herpes simplex virions, one (VP22) transports the mRNA to uninfected cells for expression prior to viral infection.* Proceedings of the National Academy of Sciences of the United States of America, 2002. **99**(12): p. 8318-8323.

69. Schwarze, S.R., et al., *In vivo protein transduction: Delivery of a biologically active protein into the mouse.* Science, 1999. **285**(5433): p. 1569-1572.
70. Fawell, S., et al., *Tat-mediated delivery of heterologous proteins into cells.* Proceedings of the National Academy of Sciences of the United States of America, 1994. **91**(2): p. 664-8.
71. Wender, P.A., et al., *The design, synthesis, and evaluation of molecules that enable or enhance cellular uptake: peptoid molecular transporters.* Proceedings of the National Academy of Sciences of the United States of America, 2000. **97**(24): p. 13003-13008.
72. Mitchell, D.J., et al., *Polyarginine enters cells more efficiently than other polycationic homopolymers.* Journal of Peptide Research, 2000. **56**(5): p. 318-325.
73. Chen, L. and S.D. Harrison, *Cell-penetrating peptides in drug development: enabling intracellular targets.* Biochemical Society Transactions, 2007. **35**(4): p. 821-825.
74. Pittet, M.J., et al., *Labeling of immune cells for in vivo imaging using magnetofluorescent nanoparticles.* Nature Protocols, 2006. **1**(1): p. 73-79.
75. Josephson, L., et al., *High-Efficiency Intracellular Magnetic Labeling with Novel Superparamagnetic-Tat Peptide Conjugates.* Bioconjugate Chemistry, 1999. **10**(2): p. 186-191.
76. Wadia, J.S. and S.F. Dowdy, *Transmembrane delivery of protein and peptide drugs by TAT-mediated transduction in the treatment of cancer.* Advanced Drug Delivery Reviews, 2005. **57**(4): p. 579-596.
77. Snyder, E.L. and S.F. Dowdy, *Recent advances in the use of protein transduction domains for the delivery of peptides, proteins and nucleic acids in vivo.* Expert Opinion on Drug Delivery, 2005. **2**(1): p. 43-51.
78. Glover, D.J., H.J. Lipps, and D.A. Jans, *Towards safe, non-viral therapeutic gene expression in humans.* Nature Reviews Genetics, 2005. **6**(4): p. 299-310.
79. Eguchi, A., et al., *Protein transduction domain of HIV-1 Tat protein promotes efficient delivery of DNA into mammalian cells.* Journal of Biological Chemistry, 2001. **276**(28): p. 26204-26210.
80. Tunnemann, G., et al., *Cargo-dependent mode of uptake and bioavailability of TAT-containing proteins and peptides in living cells.* The FASEB journal, 2006. **20**(11): p. 1775-84.
81. Meade, B.R. and S.F. Dowdy, *Exogenous siRNA delivery using peptide transduction domains/cell penetrating peptides.* Advanced Drug Delivery Reviews, 2007. **59**(2-3): p. 134-140.
82. Fischer, R., et al., *Break on through to the other side-biophysics and cell biology shed light on cell-penetrating peptides.* ChemBioChem, 2005. **6**(12): p. 2126-2142.
83. Gump, J.M. and S.F. Dowdy, *TAT transduction: the molecular mechanism and therapeutic prospects.* Trends in Molecular Medicine, 2007. **13**(10): p. 443-448.
84. Zaro, J.L. and W.-C. Shen, *Cytosolic delivery of a p16-peptide oligoarginine conjugate for inhibiting proliferation of MCF7 cells.* Journal of Controlled Release, 2005. **108**(2-3): p. 409-417.

85. Silhol, M., et al., *Different mechanisms for cellular internalization of the HIV-1 Tat-derived cell penetrating peptide and recombinant proteins fused to Tat.* European Journal of Biochemistry, 2002. **269**(2): p. 494-501.
86. Pacifici, R.E. and K.J.A. Davies, *Protein, lipid and DNA repair systems in oxidative stress: the free-radical theory of aging revisited.* Gerontology, 1991. **37**(1-3): p. 166-80.
87. Davies, K.J.A., *Oxidative stress: the paradox of aerobic life.* Biochemical Society Symposia, 1995. **61**(Free Radicals and Oxidative Stress: Environment, Drugs and Food Additives): p. 1-31.
88. Mezzetti, A., et al., *Systemic oxidative stress and its relationship with age and illness. Associazione Medica "Sabin".* Journal of the American Geriatrics Society, 1996. **44**(7): p. 823-7.
89. Stohs, S.J., *Synthetic pro-oxidants: Drugs, pesticides and other environmental pollutants.* Oxidative Stress and Antioxidant Defenses in Biology, 1995: p. 117-80.
90. Dore, S. and S.H. Snyder, *Neuroprotective action of bilirubin against oxidative stress in primary hippocampal cultures.* Annals of the New York Academy of Sciences, 1999. **890**(Neuroprotective Agents): p. 167-172.
91. Maharaj, D.S., B.D. Glass, and S. Daya, *Melatonin: New places in therapy.* Bioscience Reports, 2007. **27**(6): p. 299-320.
92. Rodriguez, M.C., et al., *Beneficial effects of creatine, CoQ10, and lipoic acid in mitochondrial disorders.* Muscle & Nerve, 2007. **35**(2): p. 235-242.
93. Strazzullo, P. and J.G. Puig, *Uric acid and oxidative stress: relative impact on cardiovascular risk.* Nutrition, Metabolism & Cardiovascular Diseases, 2007. **17**(6): p. 409-414.
94. Liebler, D.C. and T.D. McClure, *Antioxidant reactions of b-carotene: identification of carotenoid-radical adducts.* Chemical Research in Toxicology, 1996. **9**(1): p. 8-11.
95. Yabe, Y., et al., *Hepatocyte-specific distribution of catalase and its inhibitory effect on hepatic ischemia/reperfusion injury in mice.* Free Radical Research, 1999. **30**(4): p. 265-274.
96. Atalla, S.L., et al., *Influence of oxygen-derived free radical scavengers on ischemic livers.* Transplantation, 1985. **40**(6): p. 584-90.
97. Nauta, R.J., et al., *Oxygen-derived free radicals in hepatic ischemia and reperfusion injury in the rat.* Surgery, gynecology & obstetrics, 1990. **171**(2): p. 120-5.
98. Jadot, G., et al., *Clinical pharmacokinetics and delivery of bovine superoxide dismutase.* Clinical pharmacokinetics, 1995. **28**(1): p. 17-25.
99. Mikawa, K., et al., *Attenuation of hyperoxic lung injury in rabbits with superoxide dismutase: effects on inflammatory mediators.* Acta Anaesthesiologica Scandinavica, 1995. **39**(3): p. 317-22.
100. Doerschuk, C.M., M.F. Allard, and M.J. Oyarzun, *Evaluation of reexpansion pulmonary edema following unilateral pneumothorax in rabbits and the effect of superoxide dismutase.* Experimental Lung Research, 1990. **16**(4): p. 355-67.
101. Flick, M.R., et al., *Catalase prevents increased lung vascular permeability during air emboli in unanesthetized sheep.* Journal of Applied Physiology, 1988. **64**(3): p. 929-35.

102. Parizada, B., M.M. Werber, and A. Nimrod, *Protective effects of human recombinant MnSOD in adjuvant arthritis and bleomycin-induced lung fibrosis.* Free Radical Research Communications, 1991. **15**(5): p. 297-301.
103. Kawada, T., et al., *Pretreatment with catalase or dimethyl sulfoxide protects alloxan-induced acute lung edema in dogs.* Journal of Applied Physiology, 1992. **73**(4): p. 1326-33.
104. Breuer, R., et al., *Superoxide dismutase inhibits radiation-induced lung injury in hamsters.* Lung, 1992. **170**(1): p. 19-29.
105. Wright, S.E., D.A. Baron, and J.E. Heffner, *Intravenous eugenol causes hemorrhagic lung edema in rats: Proposed oxidant mechanisms.* Journal of Laboratory and Clinical Medicine, 1995. **125**(2): p. 257-64.
106. Petelin, M., et al., *Local delivery of liposome-encapsulated superoxide dismutase and catalase suppress periodontal inflammation in beagles.* Journal of Clinical Periodontology, 2000. **27**(12): p. 918-925.
107. Muzykantov, V.R., *Targeting of superoxide dismutase and catalase to vascular endothelium.* Journal of Controlled Release, 2001. **71**(1): p. 1-21.
108. Veronese, F.M., et al., *Polyethylene glycol-superoxide dismutase, a conjugate in search of exploitation.* Advanced Drug Delivery Reviews, 2002. **54**(4): p. 587-606.
109. Fridovich, I., *Superoxide dismutases. An adaptation to a paramagnetic gas.* Journal of Biological Chemistry, 1989. **264**(14): p. 7761-4.
110. Sherman, L., et al., *Nucleotide sequence and expression of human chromosome 21-encoded superoxide dismutase mRNA.* Proceedings of the National Academy of Sciences of the United States of America, 1983. **80**(18): p. 5465-9.
111. Ho, Y.S. and J.D. Crapo, *Isolation and characterization of complementary DNAs encoding human manganese-containing superoxide dismutase.* FEBS Letters, 1988. **229**(2): p. 256-60.
112. Tainer, J.A., et al., *Determination and analysis of the 2 .ANG. structure of copper,zinc superoxide dismutase.* Journal of Molecular Biology, 1982. **160**(2): p. 181-217.
113. Fielden, E.M., et al., *The mechanism of action of superoxide dismutase from pulse radiolysis and electron paramagnetic resonance. Evidence that only half the active sites function in catalysis.* Biochemical Journal, 1974. **139**(1): p. 49-60.
114. Klug-Roth, D., I. Fridovich, and J. Rabani, *Pulse radiolytic investigations of superoxide catalyzed disproportionation. Mechanism for bovine superoxide dismutase.* J Am Chem Soc FIELD Full Journal Title:Journal of the American Chemical Society, 1973. **95**(9): p. 2786-90.
115. Rotilio, G., R.C. Bray, and E.M. Fielden, *Pulse radiolysis study of superoxide dismutase.* Biochimica et Biophysica Acta, Enzymology, 1972. **268**(2): p. 605-9.
116. Rotilio, G., et al., *Metal sites of copper proteins. III. Symmetry of copper in bovine superoxide dismutase and its functional significance.* Biochemistry, 1972. **11**(11): p. 2187-92.
117. Hart, P.J., et al., *A Structure-Based Mechanism for Copper-Zinc Superoxide Dismutase.* Biochemistry, 1999. **38**(7): p. 2167-2178.

118. Rypniewski, W.R., et al., *Crystal structure of reduced bovine erythrocyte superoxide dismutase at 1.9 .ANG. resolution.* Journal of Molecular Biology, 1995. **251**(2): p. 282-96.
119. Kumar, M., et al., *Highly permeable polymeric membranes based on the incorporation of the functional water channel protein Aquaporin Z.* Proceedings of the National Academy of Sciences of the United States of America, 2007. **104**(52): p. 20723-8.
120. Nardin, C., et al., *Polymerized ABA Triblock Copolymer Vesicles.* Langmuir, 2000. **16**(3): p. 1035-1041.
121. Williams, G., et al., *Further considerations of nonsymmetrical dielectric relaxation behavior arising from a simple empirical decay function.* Transactions of the Faraday Society, 1971. **67**(Pt. 5): p. 1323-35.
122. Rigler, P. and W.K. Meier, *Encapsulation of fluorescent molecules by functionalized polymeric nanocontainers: investigation by confocal fluorescence imaging and fluorescence correlation spectroscopy.* Journal of the American Chemical Society, 2006. **128**(1): p. 367-373.
123. Williams, P.A., *Physical techniques for the study of food biopolymers. S. B. Ross-Murphy*. International Journal of Food Science and Technology. Vol. 29. 1994. 616.
124. Michel, E., et al., *Kinetics properties of Cu,Zn-superoxide dismutase as a function of metal content. [Erratum to document cited in CA143:224756].* Archives of Biochemistry and Biophysics, 2005. **444**(1): p. 76.
125. Bermudez, H., et al., *Molecular Weight Dependence of Polymersome Membrane Structure, Elasticity, and Stability.* Macromolecules, 2002. **35**(21): p. 8203-8208.
126. Rajagopalan, P.T.R., et al., *Interaction of dihydrofolate reductase with methotrexate: Ensemble and single-molecule kinetics.* Proceedings of the National Academy of Sciences of the United States of America, 2002. **99**(21): p. 13481-13486.
127. Comellas-Aragones, M., et al., *A virus-based single-enzyme nanoreactor.* Nature Nanotechnology, 2007. **2**(10): p. 635-639.
128. Flomenbom, O., et al., *Stretched exponential decay and correlations in the catalytic activity of fluctuating single lipase molecules.* Proceedings of the National Academy of Sciences of the United States of America, 2005. **102**(7): p. 2368-2372.
129. Roeffaers, M.B.J., et al., *Single-molecule fluorescence spectroscopy in (bio)catalysis.* Proceedings of the National Academy of Sciences of the United States of America, 2007. **104**(31): p. 12603-12609.
130. Boukobza, E., A. Sonnenfeld, and G. Haran, *Immobilization in surface-tethered lipid vesicles as a new tool for single biomolecule spectroscopy.* Journal of Physical Chemistry B, 2001. **105**(48): p. 12165-12170.
131. Hough, M.A. and S.S. Hasnain, *Crystallographic structures of bovine copper-zinc superoxide dismutase reveal asymmetry in two subunits: Functionally important three and five coordinate copper sites captured in the same crystal.* Journal of Molecular Biology, 1999. **287**(3): p. 579-592.
132. Palivan, C.G., H. Palivan, and B.A. Goodman, *Characterization by EPR spectroscopy of the coordination environment of copper in superoxide dismutase from horseradish (Armoracia rusticana Gaertn.).* Proceedings of the

Royal Society of Edinburgh, Section B: Biological Sciences, 1994. **102**(Oxygen and Environmental Stress in Plants): p. 273-7.
133. Palivan, C.G. and B.A. Goodman, *Determination of the copper coordination environment in superoxide dismutases (SODs) and complexes with SOD activity using molecular mechanics force field calculations and electron paramagnetic resonance spectroscopy.* Recent Research Developments in Inorganic & Organometallic Chemistry, 2001. **1**: p. 141-159.
134. Schweiger, A. and G. Jeschke, *Principles of Pulse Electron Paramagnetic Resonance Spectroscopy*. 2001. 572 pp.
135. Greenfield, N.J., *Applications of circular dichroism in protein and peptide analysis.* Trends in Analytical Chemistry, 1999. **18**(4): p. 236-244.
136. Ellerby, L.M., et al., *Copper-Zinc Superoxide Dismutase: Why Not pH-Dependent?* Journal of the American Chemical Society, 1996. **118**(28): p. 6556-6561.
137. Fridovich, I., *Superoxide anion radical (O2-.), superoxide dismutases, and related matters.* The Journal of biological chemistry, 1997. **272**(30): p. 18515-7.
138. Ranquin, A., et al., *Therapeutic Nanoreactors: Combining Chemistry and Biology in a Novel Triblock Copolymer Drug Delivery System.* Nano Letters, 2005. **5**(11): p. 2220-2224.
139. Gus'kova, R.A., et al., *Permeability of bilayer lipid membranes for superoxide (O2-.) radicals.* Biochimica et Biophysica Acta, Biomembranes, 1984. **778**(3): p. 579-85.
140. Takahashi, M. and K. Asada, *Superoxide anion permeability of phospholipid membranes and chloroplast thylakoids.* Archives of Biochemistry and Biophysics, 1983. **226**(2): p. 558-66.
141. Broz, P., et al., *Toward Intelligent Nanosize Bioreactors: A pH-Switchable, Channel-Equipped, Functional Polymer Nanocontainer.* Nano Letters, 2006. **6**(10): p. 2349-2353.
142. Vriezema, D.M., et al., *Vesicles and polymerized vesicles from thiophene-containing rod-coil block copolymers.* Angewandte Chemie, International Edition, 2003. **42**(7): p. 772-776.

8 Curriculum vitae

Personal Data	
Name, First Name:	Axthelm, Fabian
Adress:	Am Laeufelberg 3
	79588 Egringen
Email:	Fabian.Axthelm@unibas.ch
Date of birth:	16. March 1979
Marital status:	married, 1 children
Nationality:	German
Languages:	English, Russian

Academic Education	
07/2004 – 072008	PhD in recombinant expression of peptide polymers for drug delivery/ development and test of an antioxidant nanoreactor, Prof. W. Meier, Dr. C.G. Palivan, **Phil.- Nat. Faculty, University of Basel, Switzerland**
01/2003 – 06/2004	post graduate studies in protein folding and channel protein characterization with Prof. A. Engel, Dr. M. Duckely, **Biozentrum, Basel,** 2nd diploma thesis
10/1998 – 12/2002	graduate studies in biotechnology, **University of applied sciences, Jena, Germany,** 1st diploma thesis in Roche on improvement and validation of recombinant carotenoid production

Internship

03/2001 – 08/2001	student apprentice in recombinant expression of pharmaceutical active compounds, **Hans Knöll Institute, Jena, Germany**

Education

08/1985 – 07/1997	**Geschwister- Scholl- Gymnasium, Zeitz, Germany**

Advanced Training

2005	Workshops „Leading Style“ and „Chairmanship and Negotiation“,**Institute of Organization Development, University of Basel, Switzerland**
04/2005 – 07/2005	workshop „business start-up“, **IFJ Institut für Jungunternehmen, St. Gallen, Switzerland**

Research Expertise

cell cultures:	shake flask, batch, fed batch, continuous culture
expression:	gene synthesis, cloning, SDS-Page, Western-Blott, Dialysis, ELISA, SEC,
analysis:	FRET, FCS, CLSM, CD, UV-VIS, Pulse Radiolysis

IT Skills

operating systems:	Linux, Windows

Additional knowledge and activities

University duties:	guiding of student apprentice and diploma students
Complimentary work:	vice president of SC Novartis Rosental Kayak Club

Publications

Palivan, C.G.; Verbert, C.; Axthelm, F.; Meier, W. **Responsive self-assembled nanostructures.** Nanotechnology in Biology and Medicine (2007), 32/1- 32/26

Duckely, M.; Oomen, C.; Axthelm, F.; Van Gelder, P.; Waksman, G.; Engel, A. **The VirE1VirE2 complex of Agrobacterium tumefaciens interacts with single-stranded DNA and forms channels.** Molecular Microbiology (2005), 58(4), 1130-1142.

Jacob, S. S.; Axthelm, F.; Hohn, B.; Duckely, M. **Mutational analysis of the channel forming protein VirE2 of Agrobacterium tumefaciens.** Biol. Plant-Microbe Interact. (2004), 4 518-520.

Krieger, F.; Fierz, B.; Axthelm, F.; Joder, K.; Meyer, D.; Kiefhaber, T. **Intrachain diffusion in a protein loop fragment from carp parvalbumin.** Chemical Physics (2004), 307(2-3), 209-215.